The Validity of Optical Properties as Tracers of Terrigenous Dissolved Organic Carbon during Extensive Remineralization in Coastal Waters

Yuan Chen[1,*], Patrick Martin[1,*], and Yongli Zhou[1,†]

[1] Asian School of the Environment, Nanyang Technological University, 639798, Singapore

[†]Present address: Marine Biological Laboratory, Woods Hole, MA 02543, USA

[*]Corresponding author:

Yuan Chen (yuan006@e.ntu.edu.sg) and Patrick Martin (pmartin@ntu.edu.sg)

Key Points:

- Chromophoric dissolved organic matter removal is more than terrestrial dissolved organic carbon (tDOC) remineralization in coastal water.
- Commonly used optical properties can quantify percent tDOC in natural environment but with different sensitivity.
- None of the optical properties can indicate the extent of tDOC remineralization from natural biogeochemical processing.

Abstract

Terrestrial dissolved organic carbon (tDOC) is significant for coastal carbon cycling, and spectroscopy of chromophoric and fluorescent dissolved organic matter (CDOM, FDOM) is widely used to study tDOC cycling. However, CDOM and FDOM are often amongst the more labile components of tDOC. Because few studies have compared spectroscopy to measurements of both bulk tDOC concentration and tDOC remineralization, it remains unclear how accurately CDOM and FDOM actually trace tDOC in coastal waters when tDOC undergoes extensive remineralization. We collected a 4-year coastal timeseries in Southeast Asia, where tropical peatlands provide a large tDOC input. A carbon stable isotope mass balance shows that on average 56% of tDOC was remineralized upstream of our site, while 77% of CDOM was bleached. Despite this extensive tDOC remineralization and preferential CDOM loss, optical properties could still reliably quantify tDOC. CDOM spectral slope properties, such as $S_{275–295}$, are exponentially related to tDOC; these are highly sensitive tDOC tracers at low, but not at high, tDOC concentrations. Other properties are linearly related to tDOC, and both specific ultraviolet absorbance ($SUVA_{254}$) and DOC-normalized fluorescence intensity may be suitable to quantify tDOC over a wider range of concentrations. However, the optical properties did not show consistent changes with the extent of tDOC remineralization. Our data support the validity of CDOM and FDOM spectroscopy to trace tDOC across coastal gradients even after the majority of tDOC has been remineralized, but they also show that these measurements may not provide direct information about the degree of natural tDOC processing.

1 Introduction

Annually around 0.25 Pg C of terrestrial dissolved organic carbon (tDOC) are transported from land to ocean, playing an important role in global and especially coastal carbon cycling (Ciais et al., 2013; Dai et al., 2012; Raymond & Spencer, 2015). A large fraction of tDOC is remineralized in ocean margin environments (Bélanger et al., 2006; Letscher et al., 2011; Painter et al., 2018). For instance, it is reported that 40%–70% of tDOC is remineralized on the Louisiana Shelf, in the Eurasian Arctic Shelf Sea and in the Sunda Shelf Sea before reaching the open ocean (Fichot & Benner, 2014; Kaiser et al., 2017; Zhou et al., 2021). The remineralization results in the formation of dissolved inorganic carbon (DIC) along with transformation of nutrient elements, thus causing ocean acidification (Capelle et al., 2020; Semiletov et al., 2016; Wit et al., 2018; Zhou et al., 2021)

and influencing nutrient distributions (Alling et al., 2012; Qualls & Richardson, 2003; Vähätalo & Zepp, 2005). In addition, a fraction of tDOC—chromophoric dissolved organic matter (CDOM) can absorb light, causing light attenuation in natural waters and affecting primary productivity and other biological activities (Aksnes et al., 2009; Martin et al., 2021; Urtizberea et al., 2013).

Since terrestrial dissolved organic matter (tDOM) is rich in CDOM and fluorescent DOM (FDOM), absorbance and fluorescence spectroscopy are widely exploited to trace tDOC in aquatic environments, due to their high sensitivity and ease of measurement (Bauer & Bianchi, 2011; Coble, 2007; Dittmar, 2015; Stedmon & Nelson, 2015). The most commonly used optical properties (Table 1) include absorption coefficients (a_λ, m^{-1}), CDOM spectral slopes (such as $S_{275–295}$, nm^{-1}) and the CDOM spectral slope ratio ($S_R=S_{275–295}/S_{350–400}$), specific ultraviolet absorbance ($SUVA_{254}$, L mg-C^{-1} m^{-1}), the fluorescence index (FI) and the humification index (HIX).

Table 1. Description of widely used optical properties indicating sources and compositions of DOM.

Optical property	**Provided information**	**Reference**
a_λ (m^{-1})	Represents CDOM concentration, often linearly correlated to DOC and lignin phenol concentrations in different aquatic environments	Fichot and Benner (2011); Hernes and Benner (2003); Osburn et al. (2016); Vantrepotte et al. (2015)
$S_{275–295}$ (nm^{-1})	Negatively correlated to DOM apparent molecular weight, exhibits exponential relationship with concentration of lignin phenols	Del Vecchio and Blough (2002); Fichot and Benner (2012); Helms et al. (2008)
S_R	Higher values indicate higher content of low apparent molecular weight components in DOM; increases upon photo exposure	Helms et al. (2008)
$S_{320–412}$ (nm^{-1})	An indicator of freshly produced autochthonous marine DOM, strong linear correlation to DOC-specific a_λ during phytoplankton bloom	Danhiez et al. (2017)
$SUVA_{254}$ (L mg-C^{-1} m^{-1})	Shows linear relationship with aromaticity of DOM	Cartisano et al. (2018); Chin et al. (1994); Hur et al. (2006); Weishaar et al. (2003)
FI	DOM is likely to be terrestrial when FI<1.4, while is more marine-sourced with higher FI	Cory et al. (2010); McKnight et al. (2001)
HIX	An indicator of content of humic substances or extent of humification in DOM, higher values corresponds to higher humification level	Ohno (2002)
BIX	An indicator of autochthonous biological activity, high values (>1) indicate dominance of aquatic DOM	Huguet et al. (2009)

Typically, tDOC is characterized by high values for a_λ, $SUVA_{254}$ and HIX, and low values for $S_{275–295}$, S_R and FI (Gandois et al., 2014; Huguet et al., 2009; Kida et al., 2018; Stedmon et al., 2011). In addition, parallel factor analysis (PARAFAC) of FDOM spectra is commonly used to identify and quantify terrestrial fluorescent components to trace tDOC distribution in natural environments (Murphy et al., 2008; Stedmon et al., 2003). Apart from these indices of terrestrial source materials, the FDOM biological index (BIX) and more recently the CDOM spectral slope between 320 and 412 nm ($S_{320–412}$, nm^{-1}) are used as tracers for in-situ production of autochthonous DOM (Table 1).

However, while these optical properties are clearly useful, especially as qualitative markers for identifying the presence and biogeochemical cycling of tDOC, it is still often unclear how accurate they really are as tracers of total tDOC across coastal gradients where tDOC undergoes extensive remineralization. Several studies have shown that some of the optical properties (a_λ, $S_{275–295}$) are related to tDOC composition in estuarine and coastal environments, and that these optical properties can therefore be used to quantify tDOC concentration (Fichot & Benner, 2012; Fichot et al., 2016; Hernes & Benner, 2003). However, on the one hand, terrigenous CDOM and FDOM may be more labile and lost preferentially relative to bulk tDOC, especially when subject to photodegradation (Benner & Kaiser, 2011; Moran et al., 2000; Osburn et al., 2009). Yet on the other hand, tDOC itself can only be estimated from proxy measures, and comparisons between optical properties and tDOC have primarily relied on lignin phenols as a biomarker to quantify tDOC. While lignin phenols unambiguously show that tDOC is present, they are only a small fraction of the bulk tDOC (Fichot & Benner, 2012; Louchouarn et al., 2000; Osburn & Stedmon, 2011), and may also decompose more easily than bulk tDOC during remineralization, especially from photodegradation (Benner & Kaiser, 2011; Cao et al., 2018; Hernes & Benner, 2003). This is further demonstrated by the fact that lignin phenols are scarce in the open-ocean DOC pool (Hedges et al., 1997; Meyers-Schulte & Hedges, 1986; Opsahl & Benner, 1997), although molecular and carbon isotope data suggest that oceanic DOC may in fact contain more tDOC than previously recognised (Cao et al., 2018; Medeiros et al., 2016; Zigah et al., 2017). Moreover, few studies have compared the various different optical properties comprehensively to evaluate which are the most reliable for tracing tDOC in natural samples with mixed sources. Where systematic comparisons have been conducted, they have been largely based on laboratory studies using DOM from a limited range of plant, soil, or microbial sources, and subjected to purely photochemical or

purely microbial degradation experiments (Hansen et al., 2016; Lee et al., 2018). Specifically, Hansen et al. (2016) showed that individual optical properties depended on both source and DOM degradation process, with photochemical and microbial degradation often causing opposing changes. They recommended that multiple optical properties should be used to evaluate DOM sources in a qualitative perspective but did not show any quantitative information. Similarly, Lee et al. (2018) concluded that SUVA, BIX and FI are most reliable as indicators of DOM source because they are rarely affected by biogeochemical processes, but they did not derive statistical relationships between optical properties and tDOC either. While these laboratory experiments have provided important insights, we do not know how closely these results resemble what happens in the coastal environment, where the DOM pool consists of many more different sources, and physical, photochemical, and microbial processes interact in potentially complex ways (Antony et al., 2018; Karen & Mary Ann, 1999; Miller & Moran, 1997). Consequently, more environmental datasets are needed in which optical parameters can be directly compared and related to the actual tDOC concentration across a known gradient of tDOC remineralization.

In this study, we used a multi-year time series of DOC concentration, DOC and DIC carbon stable isotope composition, and DOM optical analysis from coastal Southeast Asia. Southeast Asia's extensive tropical peatlands deliver around 10% of global land–ocean DOC flux (Baum et al., 2007; Huang et al., 2017; Moore et al., 2011), while the region's archipelagic geography and monsoon-driven ocean current reversal result in long water residence times on the shelf (Mayer et al., 2022), allowing the majority of tDOC to be remineralized within the shelf sea (Wit et al., 2018; Zhou et al., 2021). We used a carbon stable isotope mass balance approach to calculate both the percentage contribution of tDOC to the bulk DOC pool (tDOC%) and the proportion of tDOC that had been remineralized to DIC. This allows us to test how accurately different optical properties can quantify tDOC%, and also to test whether any of the optical properties change purely as a function of the extent of tDOC remineralization. In addition, we compared our environmental data to results obtained from laboratory tDOC remineralization experiments to examine whether the changes in optical properties during such simplified experiments reflect the patterns we observed in our environmental data. This study not only provides a comprehensive dataset of a hotspot for carbon cycling investigation to fill the gap in global coastal carbon and optical analysis, but also proves the validity of applying spectroscopic techniques to broadly trace tDOC quantitatively in natural environment.

2 Dataset and Methods

2.1 Datasets used in the present analysis

The main dataset used in the present analysis is a multi-year time series of DOC concentration, stable carbon isotope composition, and optical properties collected in the Singapore Strait. In the Singapore Strait, the monsoon system causes a seasonal reversal of water currents (Mayer et al., 2022; Susanto et al., 2016; van Maren & Gerritsen, 2012): this causes tDOC originating from peatlands on Sumatra to be transported to our study site during the Southwest (SW) Monsoon (May to September), while water from the South China Sea with a mostly marine DOC pool is delivered during the Northeast (NE) Monsoon (November to March) (Zhou et al., 2021). The map of the study area is provided as Figure S1 in supporting information (SI). The present analysis extends this time series by one more year compared to our previous publications (Zhou et al. 2021; Martin et al. 2021), and focuses on comparing the performance of different optical properties in tracing actual tDOC in coastal environment. While our previous publications only used part of the optical dataset, mostly as supporting data to qualitatively confirm the monsoon-driven tDOC input, the present study provides a comprehensive analysis to determine how the optical properties relate quantitatively to variation in natural tDOC concentration and remineralization.

Because we lack optical data from the peatland-draining rivers on Sumatra that form the riverine endmember for our study site (Martin et al., 2022; Zhou et al., 2021), we complement our analysis using two other data sources. For CDOM absorption (as a_{440}), we calculated the discharge-weighted average for the main peatland-draining rivers based on Wit et al. (2018) and Siegel et al. (2019), detailed in Section 2.5.2. The resulting values of a_{440} and DOC follow the same CDOM-DOC relationship found for the various peatland-draining rivers in Sarawak (Figure S2; Martin et al., 2018). This indicates that the tDOC composition and optical properties are broadly similar across Southeast Asian peatlands, which is also consistent with the fact that DOC concentrations in peatland-draining rivers follow a single, strong relationship to catchment peatland cover across both Sumatra and Borneo (Rixen et al., 2022). Therefore, for the other optical properties, we used CDOM and FDOM data acquired from three expeditions in rivers in Sarawak, Borneo (Martin et al., 2018; Zhou et al., 2019). The Sarawak data were divided into three categories: peat-majority

rivers (salinity<1), with catchment peatland coverage ≥50%, non-peat-majority rivers (salinity<1), with catchment peatland coverage <50%, and Sarawak estuarine and coastal water (salinity≥1).

2.2 Singapore Strait timeseries sampling

The Singapore Strait timeseries data were collected from October 2017 to July 2021. Water samples were collected from 5-m depth at two sites in the Singapore Strait using a Niskin bottle. Sampling was undertaken monthly except during pandemic-related restrictions. The water was filtered onboard through a pre-rinsed 0.22 μm polyethersulfone membrane (Supor, Merck Millipore) with a peristaltic pump. All vials and tubes had been washed with 1 M HCl and ultrapure water (18.2 MΩ cm^{-1}). Amber borosilicate vials for DOC and optical measurements were pre-combusted at 450 °C for 4 h after washing. At each station, a depth profile of salinity and temperature was measured using a fastCTD Profiler (Valeport Ltd). The water column typically does not show stratification (Martin et al., 2022).

2.3 Sample analysis

2.3.1 Dissolved carbon and total alkalinity analysis

Triplicate DOC samples were acidified with 50% sulfuric acid, stored at +4 °C, and analysed on a Shimadzu TOC-L system with a high-salt combustion kit. For each sample, 5–7 replicate injections were performed to ensure that the coefficient of variation was less than 2%. Deep-sea water (42−45 μmol/L DOC) from the University of Miami, USA was analysed on each run (long-term mean and standard deviation from 2017–2022: 46.7 ± 4.2 μmol/L).

Dissolved inorganic carbon (DIC) was analysed on an Apollo SciTech AS-C5 DIC analyser at room temperature (22 ± 0.5°C). Each sample was measured 3−5 times to obtain a relative standard deviation less than 0.1%. Certified reference material (CRM) from Scripps Institution of Oceanography (Batch 172) or an in-house secondary standard of Singapore Strait seawater was used for calibration. The analytical precision was ±0.15%.

Total alkalinity (TA) was analysed at room temperature (22 ± 0.5 °C) on an Apollo SciTech AS-ALK2 titrator with a ROSS combination glass pH electrode (Orion 8302BNUMD), conducting the Gran titration (Gran, 1952) automatically. The titration was conducted with a 25-mL aliquot

and 0.1 M hydrochloric acid (HCl) and repeated 2−4 times for each sample. The CRM or secondary standard above was used for calibration and the analytical precision was ±0.13%.

Stable isotope ratio of DOC ($\delta^{13}C_{DOC}$) samples were stored at -20 °C, then thawed and acidified with 35 μL concentrated HCl to pH of 2−3 and analyzed at the Ján Veizer Stable Isotope Laboratory, University of Ottawa, Canada (2-sigma analytical precision of ±0.4%).

Stable isotope composition of DIC ($\delta^{13}C_{DIC}$) samples were partly analyzed at the Stable Isotope Facility, University of California, Davis using a GasBench II system with a Thermo Scientific Delta V Plus isotope-ratio mass spectrometer (analytical precision of ±0.1‰), and partly analysed in the Marine Geochemistry Laboratory, Nanyang Technological University, Singapore as described previously (Zhou et al., 2021), with analytical precision of ±0.2‰.

2.3.2 Optical analyses

Samples for CDOM and FDOM were analysed at room temperature (~22 °C) on the day of collection or after overnight storage at +4°C. CDOM absorption was measured on a Thermo Evolution 300 dual-beam spectrophotometer from 230 nm to 900 nm at 1-nm resolution in 10-cm or 2-mm quartz cuvettes with ultrapure water as a reference. They were baseline-corrected and analysed using the R package "hyperSpec" (Beleites & Sergo, 2018; Green & Blough, 1994). We calculated the following properties: a_{350} or a_{440} (m^{-1}; Green and Blough, 1994), $S_{275–295}$ (nm^{-1}; Helms et al., 2008), $S_{320–412}$ (nm^{-1}; Danhiez et al., 2017), S_R (Helms et al., 2008) and $SUVA_{254}$ (L mg-C^{-1} m^{-1}; Weishaar et al., 2003).

FDOM steady-state fluorescence excitation–emission matrices (EEMs) were measured on a HORIBA Jobin Yvon FluoroMax-4 fluorometer in a 1-cm or 3-mm quartz cuvette at excitation wavelength of 250–450 nm with 5-nm intervals and emission wavelength of 290–550 nm with 2-nm intervals, with 5 nm for both bandwidths. EEMs of ultrapure water were analyzed to record Raman and Rayleigh scattering. EEMs were processed using the Matlab drEEM toolbox (Murphy et al., 2013) to achieve inner filter effects (IFE) correction, blank subtraction, and conversion to Raman units (RU; Lawaetz & Stedmon, 2009). We calculated the fluorescence index (FI; Cory et al., 2010), humification index (HIX; Ohno, 2002) and biological freshness index (BIX; Huguet et

al., 2009). The calculations of these optical properties and the information that they are considered to provide are described in Table 1.

2.4 Photodegradation experiments

We used data from the same photodegradation experiments reported by Zhou et al. (2021) that were conducted with water samples from a peatland-draining river on Borneo (Maludam River) and from the Singapore Strait during the SW Monsoon. Although we used the same dataset as the previous publication, our purpose here is to identify whether any of the properties is quantitatively related to the extent of tDOC photochemical remineralization, which was not addressed in Zhou et al. (2021). The experimental methods are described in detail in Zhou et al. (2021); briefly, 30 mL filtered water was added into replicate cylindrical quartz cells (50 mm pathlength, 50 mm diameter) with Teflon screw caps, and irradiated under a xenon lamp with daylight optical filter in an Atlas Suntest CPS + solar simulator. Dark controls of filtered water were placed in Duran bottles fully wrapped with aluminium foil in the solar simulator. Two replicates each for light-exposed and control samples were withdrawn at each time point for DOC concentration and optical measurements.

2.5 Statistical analysis

2.5.1 Parallel factor analysis

Parallel factor analysis (PARAFAC) can partition fluorescence EEMs into underlying fluorescent components to characterize and quantify the relative contribution of different fractions (Cory & McKnight, 2005; Murphy et al., 2013; Stedmon & Bro, 2008). A total of 550 sample EEMs, including environmental data from the Singapore Strait and Sarawak, Borneo, and experimental data from photodegradation and bio-incubation for coastal seawater and Maludam water (Zhou et al., 2021; Zhou et al., 2019), were analysed by PARAFAC using the drEEM toolbox in MATLAB (Murphy et al., 2013). Eleven EEMs were excluded because they were identified as outliers by visual inspection. A five-component model was generated and validated by split-half analysis. The excitation and emission peak wavelengths of the 5 components (C1−C5) were compared with other studies (Coble, 1996; Murphy et al., 2008; Osburn et al., 2016; Stedmon & Markager, 2005a; Stedmon et al., 2003; Zhou et al., 2019) to attribute possible sources of the DOM fractions they represent (Figure S3 and Table S1). The fluorescence intensity at the excitation and emission

maximum (Fmax) is a measure of the contribution to total fluorescence and of the concentration of each DOM fraction represented by the corresponding PARAFAC component.

2.5.2 Mixing models and carbon isotope mass balance calculation

We assessed the mixing behaviour of the optical parameters across the whole salinity gradient. Moreover, we used a carbon isotope mass balance approach to calculate the amount of tDOC that has been remineralized, following the approach of previous publications (Humborg et al., 2017; Samanta et al., 2015; Su et al., 2017; Zhou et al., 2021). Specifically, we used two-endmember mixing models to estimate expected distributions of measured parameters across the salinity gradient for purely conservative mixing between a riverine and a marine endmember. We obtained riverine endmember values of DOC concentration, a_{440}, $\delta^{13}C_{DOC}$, $\delta^{13}C_{DIC}$, DIC and TA (Table S2) by taking discharge-weighted averages of data from the four main peat-draining rivers on Sumatra (the Indragiri, Kampar, Siak and Batanghari in Figure S1b) that are the most plausible sources of peatland tDOC to the Singapore Strait (Siegel et al., 2019; Siegel et al., 2009; Wit et al., 2018; Zhou et al., 2021). The resulting riverine endmember values were corroborated by the fact that the a_{440} and DOC fall onto the same CDOM–DOC relationship found for the various peatland-draining rivers in Sarawak (Figure S2; Martin et al., 2018). This suggests that peatland tDOM pools and their optical properties are quite similar across Southeast Asian peatlands, and that variation in tDOC concentration among rivers is primarily a function of catchment peatland coverage rather than reflecting differences in tDOM characteristics (Rixen et al., 2022). Since $\delta^{13}C_{DOC}$ in peatland-draining rivers of Southeast Asia mostly ranges between −30 and −28‰ (Evans et al., 2014; Gandois et al., 2014; Zhu et al., 2020), we adopted an approximated value of −29‰ as the riverine endmember. Photodegradation and combined photo-biodegradation of tDOC can cause fractionation of −1.4‰ to −5.8‰ between the original $\delta^{13}C_{DOC}$ and the produced $\delta^{13}C_{DIC}$ values (Opsahl & Zepp, 2001; Osburn et al., 2001; Spencer, Stubbins, et al., 2009). Given that peatland-derived tDOC in Southeast Asia appears to be fairly refractory to direct biodegradation but shows high photo-lability (Nichols & Martin, 2021; Zhou et al., 2021), we adopted a fractionation of −3‰, thus taking −32‰ as the $\delta^{13}C_{DIC}$ value for remineralized tDOC in our calculation. Marine endmember values were determined as averages of the measurements during late February and March, when marine water from the open South China Sea predominates in the Singapore Strait

with little tDOC presence (Figure 1). The fractional contributions of freshwater and seawater were determined from salinity.

To quantify the remaining tDOC concentration and how much tDOC had already been remineralized to DIC, we assumed that tDOC is the only source of remineralized terrigenous carbon while terrigenous POC does not make contribution, and that autochthonous DOC cycling does not influence our estimation. These assumptions are discussed in Section 4.1. The equations for the carbon isotope mass balance calculation are provided in the SI (Samanta et al., 2015; Zhou et al., 2021). Briefly, the concentration of tDOC in each sample was calculated from the measured $\delta^{13}C_{DOC}$ and DOC concentration using a two-endmember isotope mixing model. We refer to this as "remaining tDOC concentration" because it represents the fraction of the initial tDOC input that remains in form of DOC, as opposed to the fraction that has been remineralized. Based on the known stoichiometric effects of primary production, remineralization, calcium carbonate production and dissolution, and air-sea CO_2 exchange on the deviations of DIC and TA from their conservative mixing values (Zeebe & Wolf-Gladrow, 2001), and on the fractionation of $\delta^{13}C$ (Opsahl & Zepp, 2001; Osburn et al., 2001; Spencer, Aiken, et al., 2009), the amount of tDOC in a sample that has already been remineralized can be back-calculated as in other studies (Humborg et al., 2017; Samanta et al., 2015; Su et al., 2017; Zhou et al., 2021). We refer to the sum of remaining tDOC and remineralized tDOC as the "total initial tDOC concentration".

The mixing patterns of both the remaining tDOC and total initial tDOC closely resembled conservative mixing, suggesting that physical mixing still dominates the concentration changes in our sampling site and that the difference between remaining tDOC and total initial tDOC results mainly from remineralization upstream of our site. As such, using our conservative mixing model, we estimated the apparent (and actual) riverine endmember DOC concentration by extrapolating the remaining tDOC (and total initial tDOC) back to salinity 0. The errors of tDOC extrapolation were the standard deviations calculated from Monte Carlo simulation by taking all uncertainties of measurements and calculation into consideration (Table S2) and recalculating 10,000 times. Similarly, the apparent riverine endmember value of a_{440} was obtained by extrapolating our a_{440} timeseries data to salinity 0 based on the conservative mixing model. The actual riverine endmember a_{440} was obtained from the discharge-weighted average as explained in the previous paragraph. The errors of apparent and actual riverine endmember a_{440} were obtained directly from

the linear regression of a_{440} against salinity and as the standard deviation from the discharge-weighted average calculation, respectively. These riverine endmember values are presented in Table S3.

3 Results

3.1 Temporal variation of DOM optical properties in the Singapore Strait

There is a seasonal change in biogeochemistry in the Singapore Strait driven by the monsoonal current reversal. The extended timeseries data in the present study demonstrates similar seasonal patterns compared to our previous publications (Martin et al., 2022; Martin et al., 2021; Zhou et al., 2021). Here, we further examine additional optical parameters ($S_{320–412}$, FI, BIX, HIX, and C2 from PARAFAC analysis) to examine the application of spectroscopic techniques to quantify the concentration and remineralization of tDOC in natural environment directly, instead of using other proxies such as lignin phenols to represent the bulk tDOC.

During the SW Monsoon (May to September), currents carry freshwater from the east coast of Sumatra to our study site in the Singapore Strait, causing salinity to drop from approximately 33 to around 29 (Figure 1a and Figure S1a). DOC concentrations and CDOM (a_{440}) increased by, respectively, 1.2–1.7 and 2–10 times compared to other seasons, with maximum concentrations showing clear interannual variability (Figure 1b–c). $S_{275–295}$ and S_R showed the lowest values during the SW Monsoon, in the range of 0.016−0.020 nm^{-1} and 0.95−1.23, respectively (Figure 1d–e). In contrast, $SUVA_{254}$ and HIX reached peak values of higher than 3.3 L $mg\text{-}C^{-1}$ m^{-1} and 0.9, respectively (Figure 1f–g). This seasonality in the optical properties indicates a large amount of tDOC input by freshwater. During the NE Monsoon and the following early inter-monsoon season (December to March), water without much terrestrial input flows from the South China Sea to the study site, resulting in relatively high $S_{275–295}$, low S_R, low $SUVA_{254}$ and low HIX. In contrast, FI and BIX tended to have consistently low values during the SW Monsoon, respectively at around 1.4 and 0.7, but exhibited variable values in the other seasons, so that the overall seasonal contrast was less strong than that for optical properties typically associated with tDOC (Figure 1h–i). Finally, $S_{320–412}$ showed very little variation and no seasonality, with values mostly from 0.015 to 0.019 nm^{-1} (Figure 1j).

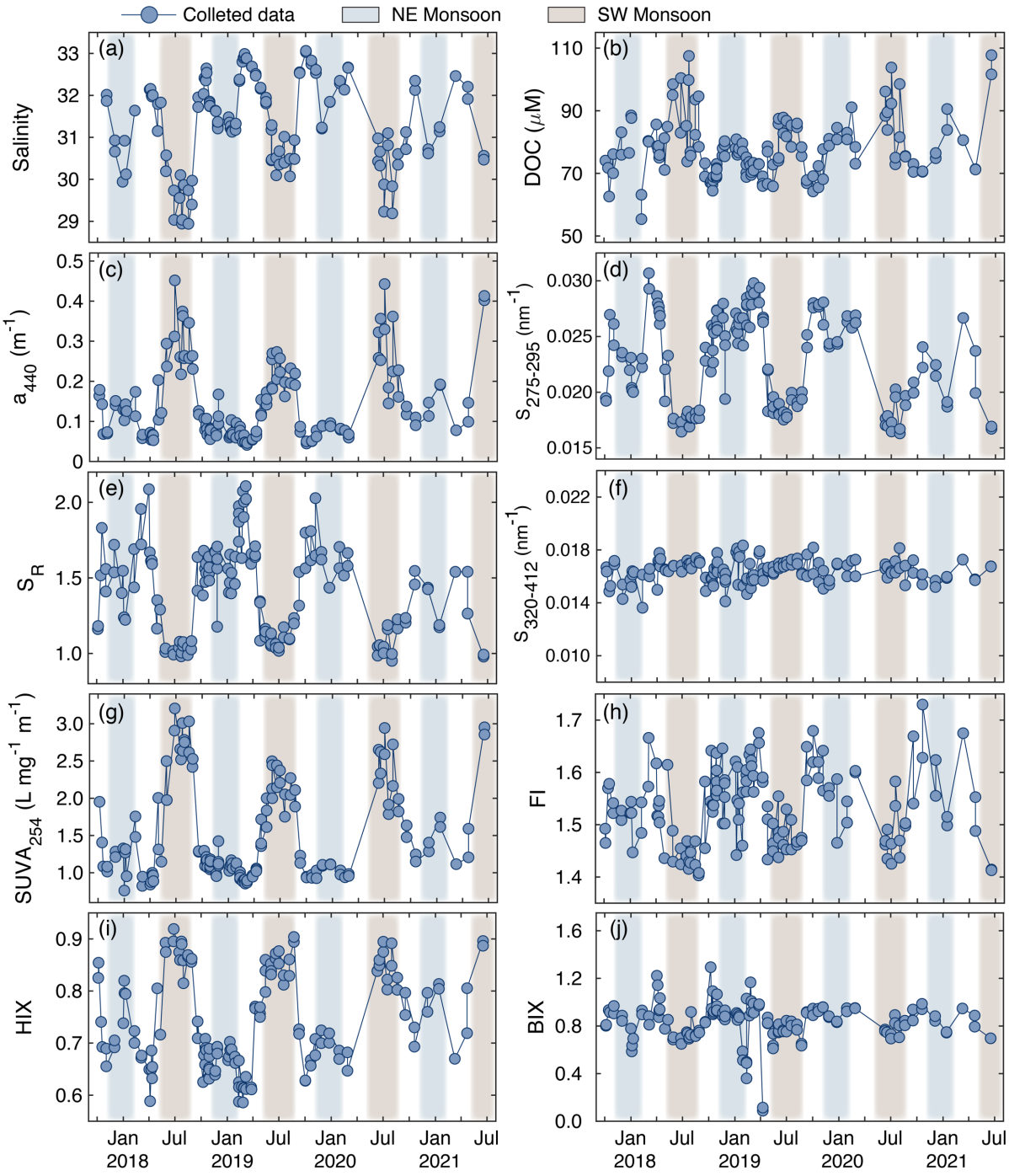

Figure 1. Timeseries data of salinity, DOC concentration and optical properties in the Singapore Strait. Data from Northeast (NE) Monsoon and Southwest (SW) Monsoon are distinguished by different shading colors. Salinity, DOC

concentration, a_{440}, $S_{275–295}$, S_R, $SUVA_{254}$, FI and HIX presented seasonal changes driven by the monsoonal current reversal, while $S_{320–412}$ and BIX showed limited or no seasonality.

3.2 Temporal variation of PARAFAC components in the Singapore Strait

Five fluorescent components (C1−C5) were identified by PARAFAC analysis (Figure S3 and Table S1), explaining 99.4% of the variability of the dataset. Among these 5 components, C1, C2 and C3 emitted mostly at visible wavelengths, which may suggest a large contribution of molecular conjugation or interaction (Chen et al., 2020; Coble, 1996; Del Vecchio & Blough, 2004a). Specifically, C1 has been identified in different water bodies (Stedmon & Markager, 2005a) and is typically associated with fulvic acid fluorophores. Emission peaks of C2 at around 430 nm with two excitation maxima at 250 nm and 430 nm have been respectively assigned as humic-like components peak A and C in previous work (Coble, 1996), and have been widely thought to represent DOM fractions with high apparent molecular weight (Jaffé et al., 2014; McKnight et al., 2001; Stedmon et al., 2003; Yamashita et al., 2008). C2 has been reported to be highly correlated with lignin phenol concentration (Yamashita et al., 2015) and is found only at low intensities in the open ocean (Murphy et al., 2008), thus is considered to be terrestrial derived. DOC-normalized C2 intensity was used previously to estimate tDOC percent contribution in the Sarawak FDOM dataset (Zhou et al., 2019). C3 also resembled the maxima characteristic of peak A but possessed a wider emission wavelength range, which has been found to be dominated by DOM derived from forest and wetland regions (Stedmon et al., 2003). Although C4 was traditionally considered related to marine humic-like material (Coble, 1996; Yamashita et al., 2015), it was related to microbial processed materials (Grunert et al., 2021; Osburn et al., 2016) and was found to have significant terrestrial signals in Southeast Asia (Harun et al., 2016; Zhou et al., 2019). In the present study, the terrestrial origin of C4 was proven by the consistent seasonal change with freshwater input caused by monsoon-driven currents. Finally, C5 showed high similarity to peak T and peak B, which are considered as protein-like fluorophores produced from microbial processes, and usually associated with fresh phytoplankton-produced DOM (Coble, 1996; Kowalczuk et al., 2013; Stedmon & Markager, 2005b; Yamashita & Tanoue, 2003; Yang & Hur, 2014).

Generally, the signals of C1−C4 exhibited similar seasonal changes during the 4 years, with high fluorescence contribution during the SW Monsoon, roughly 4−11 times greater than those during

other seasons (Figure 2a−d). This seasonality is consistent with the reported attribution of PARAFAC components mentioned above and the monsoon-driven freshwater delivery to the sampling site. There was also an interannual variability of peak values, consistent with that observed in DOC concentration, a_{440} and $SUVA_{254}$. Among these four components, their intensities followed an order of C3 > C2 > C4 > C1. In contrast, Fmax of C5 stayed within the range of 0.015−0.035 RU without obvious seasonality (Figure 2e). This suggests that there is a baseline of marine-sourced DOM in the Singapore Strait that is hardly influenced by seasonal water advection and mixing.

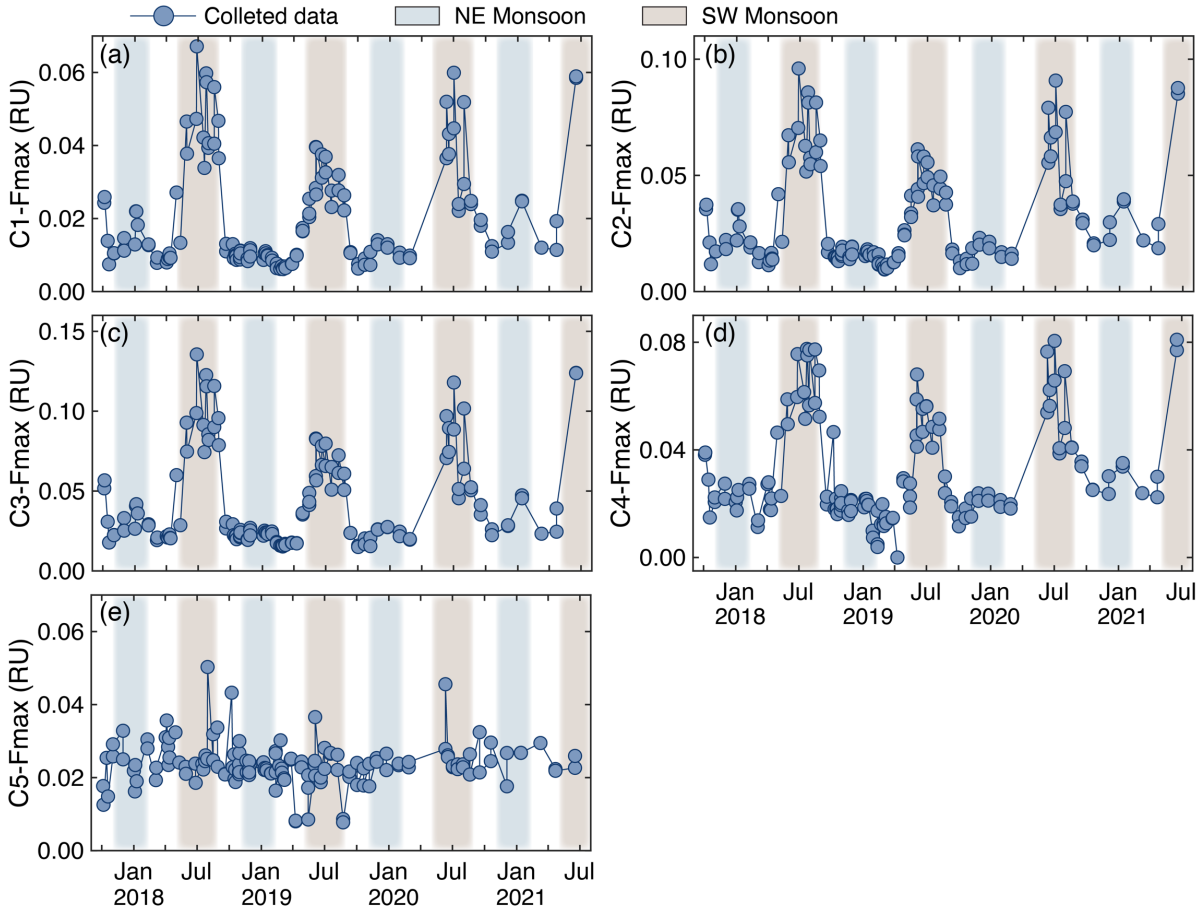

Figure 2. Timeseries data of FDOM component intensities derived from PARAFAC analysis. Components 1-4 were identified as terrestrial components as their variability was consistent with seasonal freshwater input. The highest

values were observed in SW Monsoon when tDOM is delivered from the west coast of Sumatra by water currents. Component 5, which was attributed to marine-sourced DOM, showed little variability.

3.3 Carbon isotope mass balance and preferential CDOM loss relative to tDOC

During the SW Monsoon, $\delta^{13}C$ tended to be more negative for both the DOC and DIC pool, with values mostly from -25.5‰ to -24‰ and -1.8‰ to -0.9‰, respectively (Figure 3a–b), indicating the large contribution of terrigenous carbon. Based on our carbon isotope mass balance, the remaining tDOC and total initial tDOC concentrations reached peak values of 50–60 μM and ~120 μM, respectively (Figure 3c–d). During the NE Monsoon and the following inter-monsoon seasons, in contrast, the timeseries data exhibited the most enriched $\delta^{13}C_{DIC}$ and $\delta^{13}C_{DOC}$ and the lowest values for the remaining tDOC and total initial tDOC concentrations.

Apparent conservative mixing was observed for both tDOC concentrations and CDOM absorption (a_{440}) in the Singapore Strait (Figure 3e–f). By calculating linear regressions against salinity for both remaining tDOC and total initial tDOC, we infer an apparent riverine tDOC concentration of 389±97 μmol L^{-1} and an actual riverine tDOC concentration of 814±133 μmol L^{-1}. Our actual riverine tDOC concentration is within the uncertainty range of the discharge-weighted average DOC (890 ± 159 μmol L^{-1}) reported from the four main peat-draining rivers in Sumatra that represent the most plausible source of tDOC input to Singapore (Wit et al., 2018). Our estimate is also very close (within 9%) to the value published previously based on a shorter timeseries (Zhou et al., 2021). The difference between the apparent and actual endmember tDOC concentrations indicates that, on average, 56% of the initial tDOC is remineralized before reaching our sampling site.

We quantified CDOM using the a_{440} rather than a_{350} to allow a direct comparison to the data published from Sumatra (Siegel et al., 2019; Siegel et al., 2009). CDOM absorption showed a strong linear correlation with salinity in the Singapore Strait ($r^2 = 0.76$, $p < 0.01$, Figure 3f), from which we infer an apparent riverine endmember a_{440} of 2.7 m^{-1}. This is 77% lower than the discharge-weighted riverine endmember a_{440} of 11.7 m^{-1} that we calculated based on the data in Siegel et al. (2019) and Wit et al. (2018). We therefore conclude that on average 77% of CDOM absorption is lost before reaching our sampling site. This shows that there is preferential loss of CDOM relative to tDOC, albeit not by a very large amount.

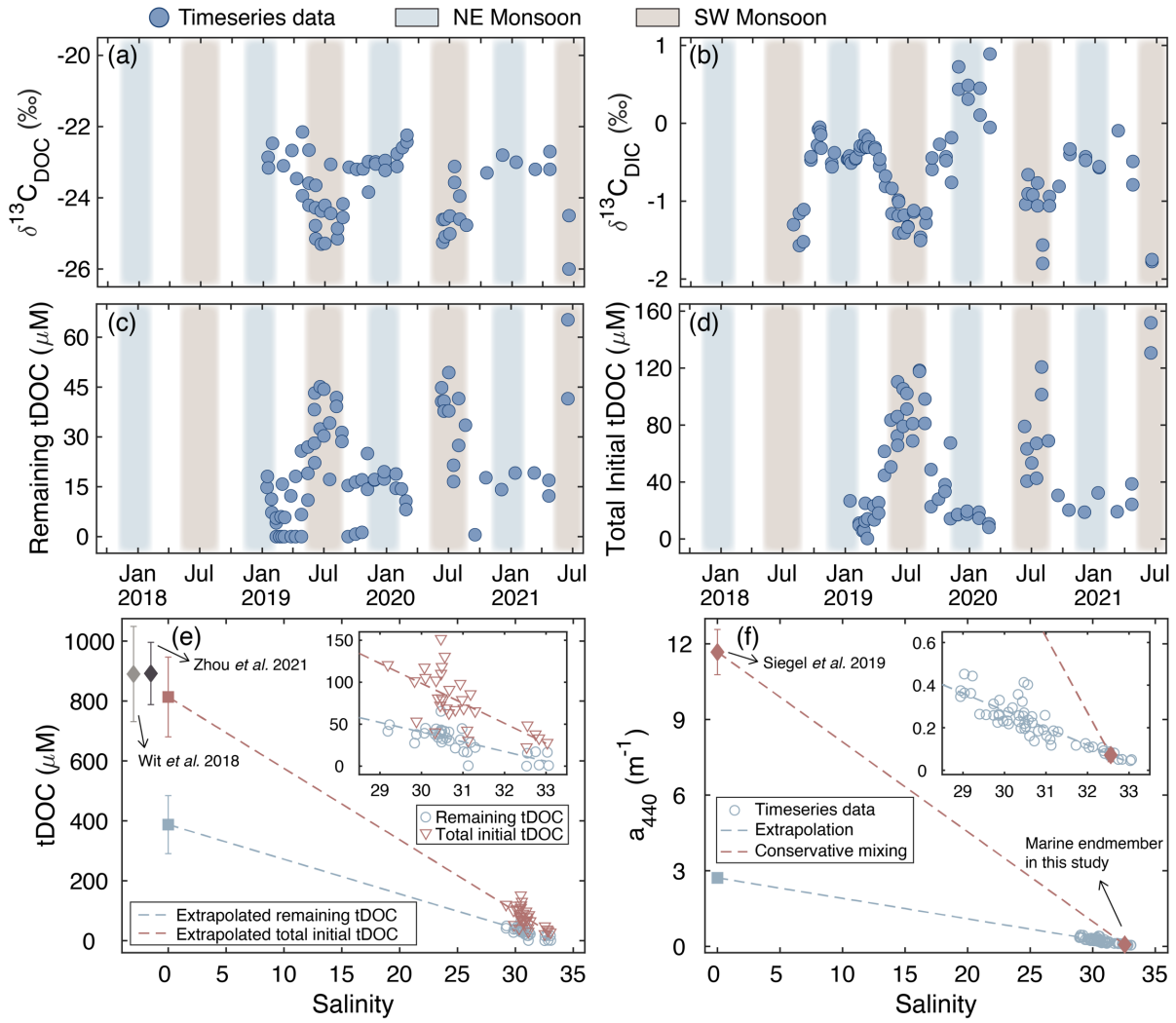

Figure 3. Timeseries data of stable carbon isotope ratios and tDOC concentrations, and mixing behaviours of tDOC and CDOM. **(a)** $\delta^{13}C_{DOC}$ and **(b)** $\delta^{13}C_{DIC}$ presented the most depleted values during the SW Monsoon due to freshwater input, while **(c)** the remaining tDOC and **(d)** total initial tDOC concentrations showed the highest values during this season. **(e)** The results of conservative mixing for tDOC concentrations suggested that on average 56% of tDOC is remineralized, while **(f)** on average 77% of CDOM is bleached before reaching our study site, showing some preferential removal of CDOM.

3.4 Mixing pattern of DOM optical properties in Singapore and Sarawak

The compiled Singapore and Sarawak carbon and optical data against salinity showed that the DOM properties at the two sites broadly fell within an overlapping range on the same mixing continuum (Figure 4). The Sarawak data showed a clear distinction for DOC concentration and for a_{440} of samples from rivers with >50% and <50% peatland in their catchments (squares in Figure

4). Clear differences between peat-majority and non-peat-majority rivers were also seen for $SUVA_{254}$, FI, HIX, and BIX, but less so for the CDOM spectral slope parameters. At low salinities (<25), corresponding to estuarine samples, high variability for DOC concentration, a_{440} and $SUVA_{254}$ was observed while the values for $S_{275–295}$, S_R, FI, HIX and BIX were more compacted (triangles in Figure 4).

Between salinities of 27–33, corresponding to more mixed coastal waters beyond the dominant influence of a single river, the values of these DOM properties for Singapore and Sarawak coastal water largely overlapped for a given salinity (triangles and circles in Figure 4). Given that the marine endmember water for Singapore and Sarawak is the southern South China Sea, the overlap in DOM properties for a given salinity suggests that the riverine endmembers from Sarawak and Sumatra have similar average tDOM composition and optical properties, as also suggested by the similar relationship of CDOM a_{440} to DOC concentration for the river data (Figure S2). Because optical properties other than a_{440} have not been measured in rivers on Sumatra, we therefore use the freshwater data from the river systems in Sarawak to provide indicative ranges of these parameters for samples of pure tDOC in our further analysis of the Singapore data below.

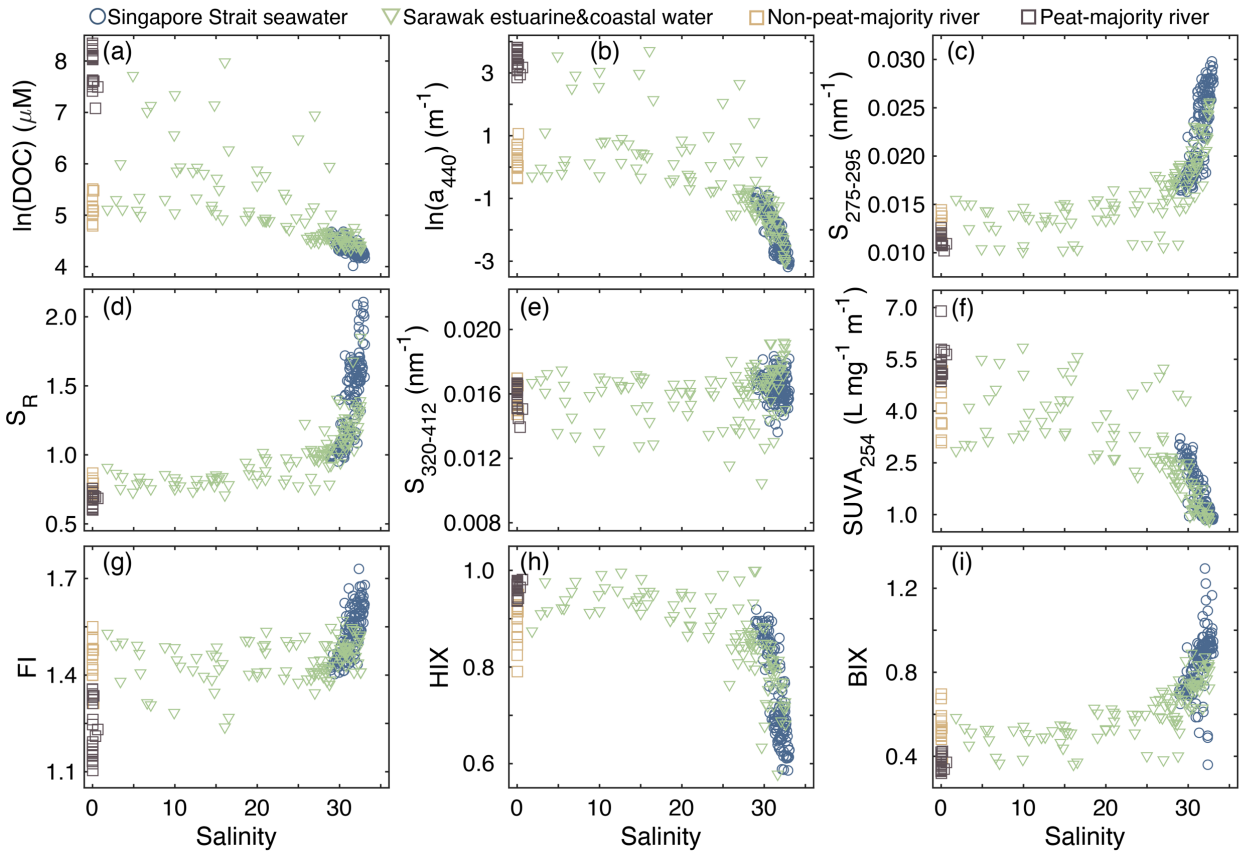

Figure 4. DOC and optical properties of coastal water in the Singapore Strait, and of rivers and estuarine/coastal waters in Sarawak (Borneo) against salinity. River data from Sarawak are distinguished by whether the catchment has >50% or <50% peatland. For all parameters, the data from the Singapore Strait fall within the same mixing continuum as coastal waters from Sarawak.

3.5 Relationships of optical properties to tDOC content

Our isotope mass balance calculation for the Singapore Strait timeseries allows us to estimate for each sample both the proportion of the bulk DOC pool that is tDOC and the amount of initially present tDOC that has been remineralized. We can therefore test how well the different optical properties are related to the tDOC content and whether they reflect the extent of prior remineralization. Given the similarity in DOM optical properties between our Singapore and Sarawak coastal water data (Figure 4 and Figure S2), we use the river data from Sarawak (at salinity 0) to provide an estimated range of values for the optical properties at 100% tDOC, prior

to experiencing remineralization in the coastal environment. The observed percentage of tDOC in coastal water is the combined result of both water mass mixing and remineralization.

Most of the optical properties showed significant relationships with the percentage of bulk DOC contributed by the remaining tDOC (tDOC%, Figure 5, statistical parameters are listed in Table 2). Specifically, a_{440} presented a strong and linear relationship with tDOC% (Figure 5a), although owing to the preferential CDOM loss (Figure 3e–f) this relationship deviated from the river data. The spectral slope properties $S_{275–295}$ and S_R showed exponential relationships with tDOC%, with both r^2 being 0.55. When the relationships were extrapolated to 100% tDOC they fell in the range of the Sarawak river data (Figure 5b–c), suggesting that these properties are applicable across the full range of tDOC%. The CDOM spectral slope $S_{320–412}$, which is indicative of fresh primary production of DOM (Danhiez et al., 2017), did not vary much throughout the whole tDOC% range (Figure 5d). $SUVA_{254}$ was linearly related to tDOC% and had the highest r^2 (0.66) of any of the optical properties (Figure 5e). Moreover, the relationship also fell within the range of the river data when extrapolated to 100% tDOC. Furthermore, compared to $S_{275–295}$ and S_R, $SUVA_{254}$ showed less scatter around the linear fitting line and possessed relatively narrower confidence and prediction intervals. For the fluorescence properties, there was a linear relationship between FI and tDOC% (Figure 5f) and the extrapolation fell within the range of collected river data, although the river values showed relatively large scatter. In contrast, HIX showed an exponential relationship with tDOC% and the relationship did not extrapolate into the range of the river data (Figure 5g). There was no relationship of BIX against tDOC% because BIX, like $S_{320–412}$, is more related to autochthonous marine DOM (Huguet et al., 2009). Finally, the DOC-normalized Fmax value of PARAFAC component 2 (C2-Fmax/DOC), which was previously used to estimate tDOC contribution in Sarawak estuaries (Zhou et al., 2019), was linearly related to tDOC%, showing similarly high r^2 (0.64) as $SUVA_{254}$ and exhibiting good consistency with the river data (Figure 5i).

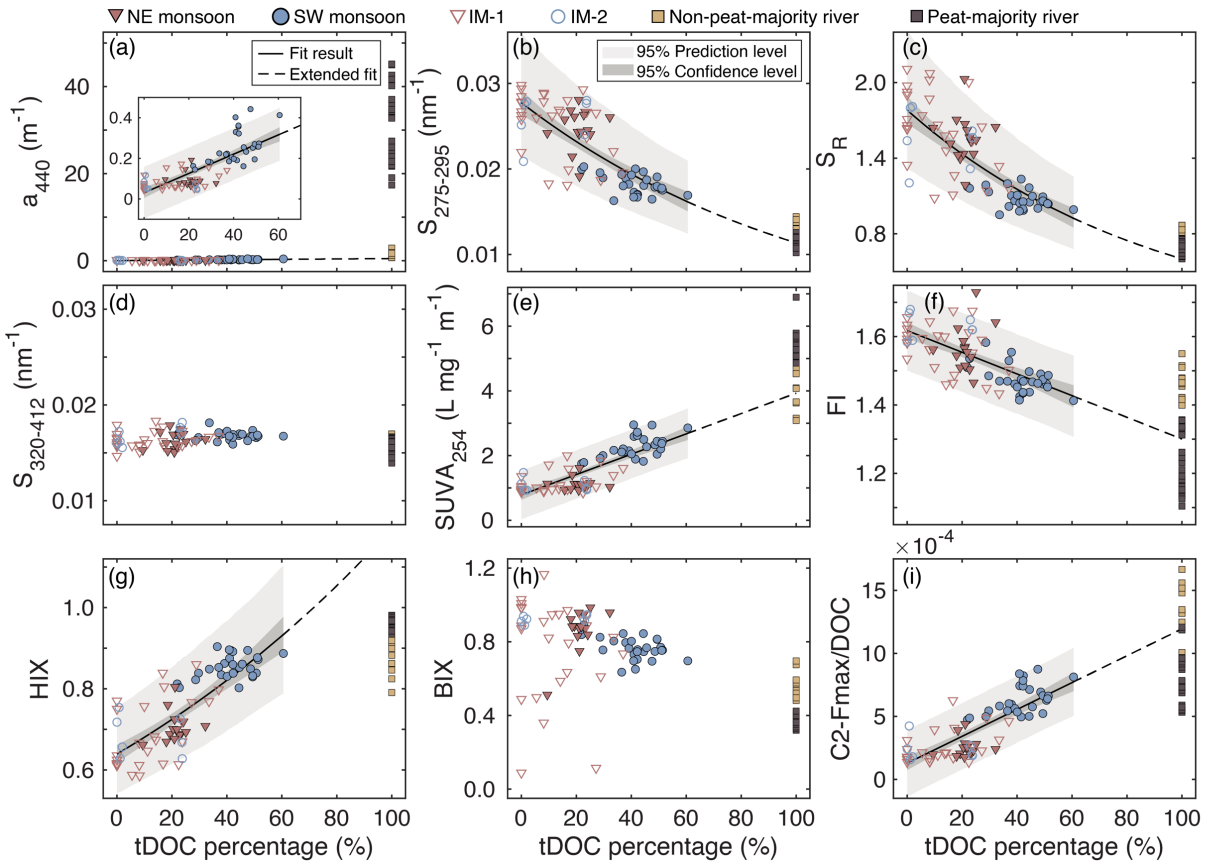

Figure 5. Relationships between optical properties and percentage contribution of tDOC to total DOC (tDOC%). The relationships were calculated only with the Singapore Strait data during NE Monsoon, Inter-Monsoon-1 (IM-1, the intermonsoon after NE Monsoon), SW Monsoon and Inter-Monsoon-2 (IM-2, the intermonsoon after SW Monsoon), but were extrapolated to 100% tDOC to compare to the reference river data from Sarawak.

Table 2. Summary of statistical relationships of optical properties with tDOC% (all N=76, $p<0.05$).

Optical property	Fitting formula	Parameter		Adjusted r^2	Consistent with river data*
		a	b		
a_{440} (m^{-1})	y = a × tDOC% + b	4.75×10^{-3}	3.08×10^{-2}	0.60	×
$S_{275–295}$ (nm^{-1})	y = exp(a× tDOC% + b)	-8.52×10^{-3}	-3.59	0.55	√
S_R	y = exp(a× tDOC% + b)	-1.06×10^{-2}	5.83×10^{-1}	0.55	√
$SUVA_{254}$ (L mg-C^{-1} m^{-1})	y = a × tDOC% + b	3.14×10^{-2}	7.86×10^{-1}	0.66	√
FI	y = a × tDOC% + b	-3.17×10^{-3}	1.62	0.45	√
HIX	y = exp(a× tDOC% + b)	6.21×10^{-3}	-4.43×10^{-1}	0.62	×
C2-Fmax/DOC	y = a × tDOC% + b	1.07×10^{-5}	1.29×10^{-4}	0.64	√

*Consistency corresponds to whether the extrapolated relationship at 100% tDOC falls within the reference river data from Sarawak: √—falls in the range, ×—falls out of the range.

3.6 Relationships of optical properties to tDOC remineralization

Our isotope mass balance showed that the tDOC had experienced a varying extent of remineralization before reaching our sampling site. Unlike the strong relationships with tDOC%, none of the optical properties were related to the extent of tDOC remineralization, even though the extent of tDOC remineralization ranged from 7% to 75% during the SW Monsoon (Figure S4). This suggests that although most of the optical properties can be used as tracers of tDOC%, they do not appear to be sensitive to the extent of tDOC remineralization in the natural environment. We restricted this analysis to include only data from the SW Monsoon as this is the only season with sufficiently large tDOC input to quantify the remineralization percentage accurately. The absolute concentration of tDOC is much lower in other seasons, and small variations in $\delta^{13}C_{DIC}$ can then result in a very large range of inferred percentage tDOC remineralization, which we consider to be inaccurate.

In contrast, most of the optical properties did show clear relationships to percentage tDOC loss in our laboratory photodegradation experiments, both with pure tDOC samples from a peatland-draining river (Maludam) and with coastal water samples from the Singapore Strait during the SW Monsoon (Figure 6). For Maludam river samples, CDOM a_{440} decreased linearly with tDOC loss while $S_{275–295}$ and S_R increased linearly by 64% and 156%, respectively (Figure 6a–c). $S_{320–412}$ and

SUVA$_{254}$ showed exponential decreases from ~0.016 to ~0.012 nm^{-1} and from ~5.2 to ~1.5 L mg-C^{-1} m^{-1}, respectively (Figure 6d–e). However, fluorescence properties showed more variability. FI first dropped by ~10% upon 30%−40% tDOC loss, after which it increased (Figure 6f). HIX always stayed at around 0.93 across the whole percent tDOC loss (Figure 6g) and BIX started to rise once tDOC loss exceeded 50% (Figure 6h). C2-Fmax/DOC exhibted a general increase of more than two times of the initial value. For the two coastal water samples from Singapore, we estimated tDOC loss by taking the prior natural tDOC remineralization (from our isotope mass balance) into account, and we conservatively assumed that all DOC lost during the incubation was tDOC, because marine DOC at our site is not very photo-sensitive (Zhou et al. 2021). Although only little DOC was remineralized in the coastal water samples, S$_{275–295}$ and S$_R$ changed by more than twofold relative to the initial values, while SUVA$_{254}$, HIX and C2-Fmax/DOC decreased linearly to a smaller degree with percent tDOC loss. S$_{320–412}$ and BIX only changed slightly.

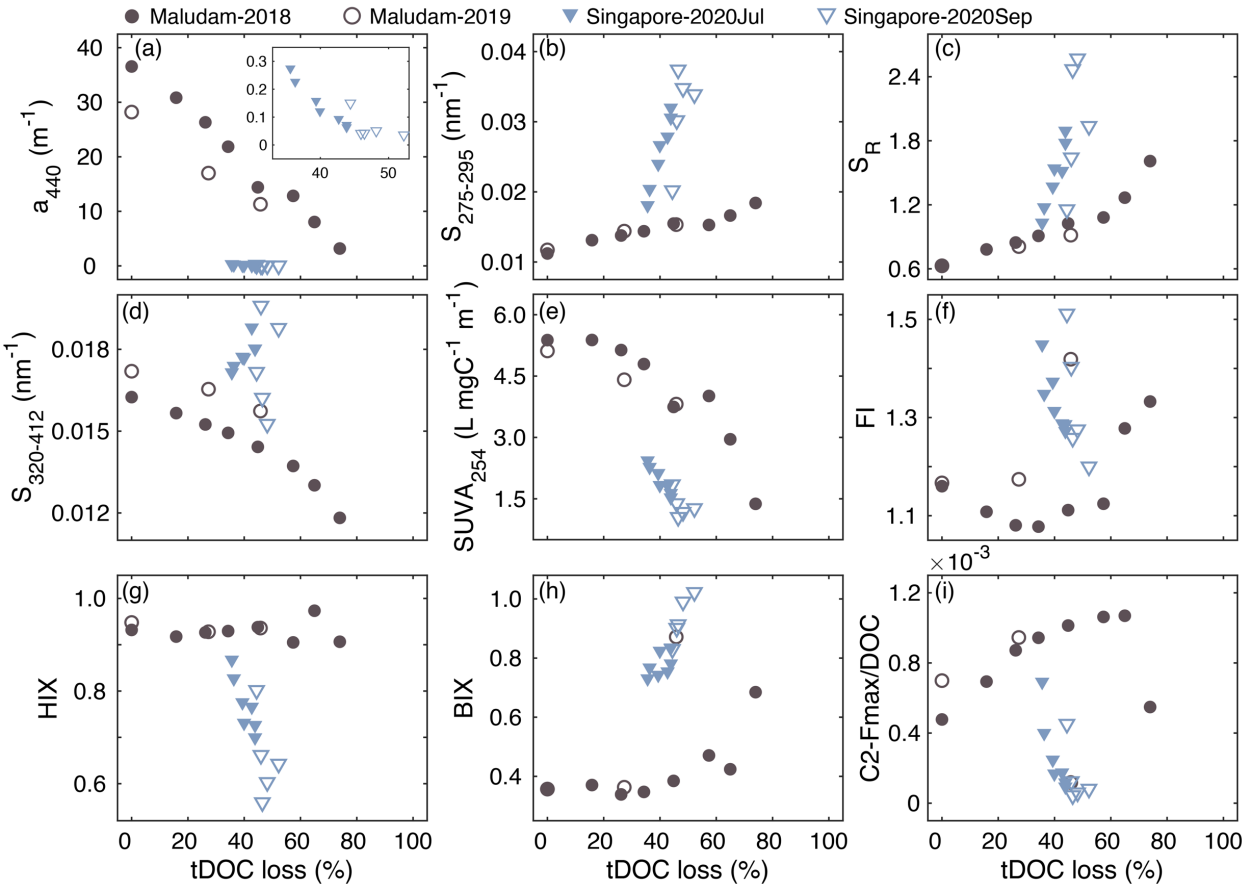

Figure 6. Changes in optical properties as a function of the percentage loss of tDOC during pure photodegradation experiments for Singapore coastal water and water from a peatland-draining river in Sarawak (Maludam River). Unlike the patterns of optical properties against percent tDOC loss in natural coastal water, most of the parameters

did present certain correlations to tDOC loss in laboratory incubation purely under photo exposure, but the correlations were different for different water types.

4 Discussion

4.1 Reliability of tDOC calculation

Carbon stable isotope measurements can provide strong insights into sources and biogeochemical processing of DOM (Alling et al., 2008; Bauer & Bianchi, 2011; Lee et al., 2020). As DOM from terrestrial source and marine environment possess distinctive carbon isotope compositions, the $\delta^{13}C_{DOC}$ values are widely used as fingerprints to distinguish DOC from different sources based on endmember mixing models (Humborg et al., 2017; Ye et al., 2018; Zhou et al., 2021). Our estimated endmember $\delta^{13}C_{DOC}$ values (Table S2) conform to the generally reported ranges of –25‰ to –32‰ and –21‰ to –22‰ for riverine and marine endmembers, respectively (Bauer, 2002; Beaupré, 2015; Gandois et al., 2014). From our estimated endmember values for $\delta^{13}C_{DOC}$ and the measured DOC concentrations in our coastal samples we could therefore use a mixing model to estimate the remaining tDOC concentration (Section 2.5.2 and Text S1.1). Besides, it is known that apart from physical mixing, biogeochemical processes including primary production/remineralization, $CaCO_3$ dissolution/calcification and CO_2 outgassing/uptake, also cause stoichiometrically constrained changes in DIC and TA, and can induce carbon isotope fractionation (Zeebe & Wolf-Gladrow, 2001). In our case, the deviations in DIC and TA are primarily caused by remineralization and $CaCO_3$ dissolution/calcification, while net CO_2 outgassing is expected within the Sunda Shelf (Kartadikaria et al., 2015; Wit et al., 2018; Zhou et al., 2021).

Several previous studies have applied the stable carbon isotope mass banlance approach to quantify the contribution of terrestrial organic matter degradation to the observed DIC and $\delta^{13}C_{DIC}$ in different regions (Humborg et al., 2017; Samanta et al., 2015; Su et al., 2020; Zhou et al., 2021) For example, it was estimated from the depletion in $\delta^{13}C_{DIC}$ that annually 4.0 Tg terrestrial organic matter is respired in the central and outer Laptev Sea in the Arctic (Humborg et al., 2017). Based on a compiled dataset including DIC, $\delta^{13}C_{DIC}$, dissolved calcium and oxygen, it was found that remineralization is the main cause of the deviation from conservative mixing in the Hooghly River

estuary in India (Samanta et al., 2015). Similarly, a mass balance calculation in the hypoxic zone of the Pearl River estuary in China demonstrated that on average 35% of the total organic matter remineralization was of terrestrial organic matter (Su et al., 2017), while the calculation in the Chesapeake Bay in the US showed that autochothounous organic matter rather than terrestrially derived organic matter dominated oxygen-consuming process (Su et al., 2020). The deviation of measured $\delta^{13}C_{DIC}$ from its conservative mixing value in our dataset (around –1‰ during SW Monsoon) is similar to the deviation observed in these previous studies, which suggests that our mass balance calculation provides robust estimates of tDOC remineralization.

The riverine endmember values in the present analysis can be considered entirely contributed by tDOC and terrigenous CDOM. On the one hand, DOM produced from phytoplankton or other microbial processes always stayed at a stedy and low level. This is demonstrated by stable $S_{320–412}$ values and low C5-Fmax largely around or even less than 0.05 RU for both coastal water and river water (Figure 4d and data not shown), both of which did not show any seasonality (Figure 1f and Figure 2e). The low $S_{320–412}$ and little signals of C5 are aligned with the annually low concentration of chlorophyll-a which is possibly caused by limited light availability (Martin et al., 2021; Morgan et al., 2020) and tidal mixing of the water column (Mayer & Pohlmann, 2014). Besides, typically >95% of the terrigenous organic carbon in Souteast Asian peatland-draining rivers is in form of DOC (Baum et al., 2007; Moore et al., 2011; Müller et al., 2015), and the small part of transported POC can probably sink and accumulate in the sediment, thus the remineralization of POC can hardly make a difference in the observed DIC and $\delta^{13}C_{DIC}$.

4.2 Preferential loss of CDOM compared to tDOC during natural remineralization

tDOC generally has a high content of chromophores, and CDOM in estuaries and coastal waters is therefore often of terrestrial origin (Asmala et al., 2012; Chen et al., 2015; Osburn et al., 2016; Santos et al., 2016). This characteristic provides the basis for using optical properties to study tDOC. Absorption coefficients (a_λ) often show strong correlations with bulk DOC concentrations in rivers, estuaries and coastal waters (Asmala et al., 2012; Fichot et al., 2016; Mann et al., 2016; Martin et al., 2018; Stedmon et al., 2011). However, we also observed preferential removal of CDOM compared to tDOC remineralization, although the difference was relatively modest (77% versus 56% loss). This finding is consistent with previous work on biological and photochemical processes of DOM for freshwater (Benner & Kaiser, 2011; Martin et al., 2018; Spencer, Stubbins,

et al., 2009) and coastal waters (Moran et al., 2000; Osburn et al., 2009). For example, the half-life time of CDOM in the Mackenzie River was estimated to be shorter than that of DOC when the river water was exposed to sunlight (Osburn et al., 2009). Similarly, removal of CDOM was found to be 21% more than that of DOC in biodegradation incubations conducted with water from a coastal estuary in Georgia after it was photo-exposed (Moran et al., 2000). Moreover, a large decrease in a_{355}/DOC ratio against salinity was observed in waters from the Middle Atlantic Bight, especially when the solar irradiance was higher (Del Vecchio & Blough, 2004b). A key mechanism driving preferential CDOM loss is likely that aromatic structures in chromophores can be partly oxidised to non-chromophoric DOC during biogeochemical processes, especially by reactive oxygen species formed under photo exposure (Cory & Kling, 2018; Del Vecchio & Blough, 2002; Vione et al., 2009). Furthermore, it is reported that photochemical reactions of specific molecules of DOM, such as aromatic amino acids, could change DOM characteristics and possibly make the products unavailable for microbes, thus inhibiting bacterial degradation processes (Amado et al., 2015). Our finding that CDOM loss is greater than tDOC loss is therefore fully consistent with previous experimental and observational research in other regions.

Pure biodegradation of Southeast Asian peatland DOM appears to be much too slow to account for the observed remineralization (Nichols & Martin, 2021), while photodegradation can remove large fractions of the tDOC and CDOM(Zhou et al., 2021). However, pure photochemical remineralization is usually fairly slow in the natural environment due to the comparatively low natural sunlight doses (Fichot & Benner, 2014; Osburn et al., 2009; Reader & Miller, 2012). Therefore, it is most likely that interactive photo-stimulated biodegradation plays an important role in tDOC remineralization and CDOM decomposition. Notably, although there is a large extent of tDOC and CDOM removal, the tDOC and CDOM concentrations still showed a pattern of conservative mixing at our study site. While this might appear to be contradictory, in fact this only indicates that physical mixing over the salinity range observed at our site occurs faster than the remineralization rate, and that the majority of the observed remineralization therefore takes place upstream of our sampling site.

4.3 Accuracy of optical properties as tracers of tDOC content in natural water

DOM optical properties have been widely measured in estuarine and coastal environments, and it is clear that they can be sensitive indicators of the presence of tDOC (Fichot & Benner, 2012;

Kaiser et al., 2017; Massicotte et al., 2017; Mizubayashi et al., 2013; Painter et al., 2018; Stedmon & Nelson, 2015). Several environmental studies have also demonstrated that some optical properties (a_λ and $S_{275–295}$) can be used to quantify tDOC concentration as calculated from lignin phenols (Fichot & Benner, 2012; Fichot et al., 2016; Hernes & Benner, 2003; Lu et al., 2016; Walker et al., 2013). However, lignin phenols are a small (typically 0.1–4% of DOC; Hernes et al., 2007; Opsahl & Benner, 1997; Osburn et al., 2016) and potentially rather labile (Cao et al., 2018; Hernes & Benner, 2003; Ronald Benner & Kaiser, 2011) fraction of tDOC, while terrigenous CDOM and FDOM may also be preferentially removed relative to bulk tDOC (Benner & Kaiser, 2011; Moran et al., 2000; Osburn et al., 2009). Specifically, both lignin and CDOM/FDOM are composed to a significant degree of aromatic moieties, which are especially photo-labile, while most aliphatic compounds are less susceptible to photodegradation (Berggren et al., 2022; Opsahl & Benner, 1998; Osburn et al., 2001; Schmitt-Kopplin et al., 1998). In contrast, aromatic components are generally more recalcitrant to microbial processes (Kang & Mitchell, 2013). These difference in reactivity can likely account for preferential removal of lignin phenols and of CDOM/FDOM relative to the bulk tDOC. For example, it was reported that the removal of lignin phenols and CDOM was more than twice as high as the loss of DOC during combined photo- and biodegradation of water from Broad River in South Carolina in the US (Benner & Kaiser, 2011). However, the degree to which optical properties are lost preferentially is likely dependent on the relative rates of different degradation processes, which are poorly quantified in natural environments. Therefore, it is still unclear how accurately these optical properties can trace total tDOC when it is also being subjected to natural remineralization processes. In the present study, we therefore used $\delta^{13}C_{DOC}$ to estimate tDOC concentration and $\delta^{13}C_{DIC}$ to estimate the extent of prior tDOC remineralization. Our results provide robust statistical evidence that all the optical properties typically used to identify tDOM are significantly related to tDOC% even when more than half of tDOC has already been remineralized (Figure 5). However, the different properties have variably strong relationships and differ in their sensitivity to tDOC in different parts of the tDOC% range.

The strong linear relationship between a_{440} and tDOC% shows that CDOM absorption coefficients can still be used to quantify tDOC in coastal water even when extensive remineralization has taken place. However, the fact that we did observe preferential removal of CDOM relative to tDOC (Figure 3e–f) underscores the fact that a_λ–tDOC relationships are sensitive to the extent of tDOM

biogeochemical degradation and must therefore change significantly across estuarine and coastal gradients. In addition, the high variability of a_{440} in estuaries can result from the mixing of seawater and different rivers with highly distinctive concentrations of tDOC and CDOM depending on the catchment coverage of peatland (Rixen et al., 2022). Caution would therefore be needed in attempting to calculate tDOC concentrations from a_λ when the range in remineralization might be large and when the riverine influence is complex.

The non-linear relationships we observed for $S_{275–295}$ and S_R with tDOC% are consistent with previous studies showing exponential relationships for $S_{275–295}$ with lignin phenol concentration (Benner et al., 2005; Fichot & Benner, 2012) and linear correlation for S_R with carbon-normalized lignin yield (Spencer et al., 2010). Besides, after extrapolating the fitting curve to salinity 0, the relationships showed good consistency with tropical peatland river data, suggesting that unlike CDOM absorption, these spectral slope-based properties maintain a constant relationship to tDOC% even as tDOC is remineralized. Based on the r^2 and confidence intervals, both $S_{275–295}$ and S_R show similar accuracy for quantifying tDOC% (Figure 5 and Table 2), resulting from the relatively steady $S_{350–400}$ across the whole salinity gradient (data not shown), consistent with previous research (Fichot & Benner, 2012). It is interesting to note that compared to $S_{275–295}$, the slope ratio S_R shows less variability at mid-salinities in the data from Sarawak, suggesting that S_R might be less sensitive to the mixing among different rivers (Figure 4d). However, in our time series data from the Singapore Strait, $S_{275–295}$ and S_R were equally well related to tDOC% (Figure 5).

$SUVA_{254}$ is usually interpreted as a measure of DOM aromaticity, as shown by ^{13}C-NMR measurements with organic matter from a variety of aquatic environments (Weishaar et al., 2003). Moreover, $SUVA_{254}$ was recently proposed as a measure to distinguish between primarily photochemically labile tDOC and bio-labile tDOC in the UniDOM biogeochemical modelling framework (Anderson et al., 2019). Our study demonstrates that $SUVA_{254}$ is linearly related to tDOC% and performs better than other CDOM measures as a quantitative tDOC tracer, given that the relationship shows less scatter (r^2 = 0.66) and narrower confidence and prediction intervals (Figure 5e). This is consistent with the robust positive relationships between $SUVA_{254}$ and the fraction of humic substances obtained from a diverse range of watersheds in the US (Spencer et al., 2012). We note that our $SUVA_{254}$–tDOC% relationship extrapolates to the lower boundary of

available river data. While the true $SUVA_{254}$ for rivers on Sumatra is not known, this result likely indicates some sensitivity of $SUVA_{254}$ to preferential CDOM loss during tDOC remineralization. Our data cannot confirm whether reduction in $SUVA_{254}$ reflects the conversion of primarily photo-labile tDOC to bio-labile structures as suggested in the UniDOM model (Anderson et al., 2019), but they do suggest that $SUVA_{254}$ can provide a good measure of tDOC in coastal environments.

The fluorescence index (FI) and humification index (HIX) are also widely used as tDOC tracers but mainly as qualitative indicators. It is suggested that when FI is less than 1.4, the DOC pool is dominated by terrestrial matter, while FI larger than 1.4 indicates an increasing dominance of microbially-derived DOC (Cory et al., 2010; McKnight et al., 2001). Our data show that FI has a clear linear relationship with tDOC% (Figure 5f), which notably contrasts with the poor relationship between FI and the proportion of humic substances in DOM reported from a river basin in eastern Thailand (Kida et al., 2018). However, the formula of FI calculation is not strictly fixed, depending on how fluorescence spectral correction is conducted (Cory & McKnight, 2005; Cory et al., 2010; McKnight et al., 2001). Additionally, it has been suggested that FI changes by at least 0.1 units when there is a source change in DOM (McKnight et al., 2001). It is clear that FI can change up to 0.3 in the Singapore Strait over a range of tDOC% from 0 (during inter-monsoon seasons) to ~60% (during the SW Monsoon). However, FI is also the most variable parameter in the river data, with some rivers having FI values similar to the inter-monsoon data from the Singapore Strait, despite carrying predominantly tDOC (Zhou et al., 2019). FI is therefore potentially less useful as a tDOC tracer than the other optical properties.

It is expected that HIX rises along with tDOC% increase because it indicates humification level, and humic substances are an important component of tDOC (Ohno, 2002; Zsolnay et al., 1999). However, similar to FI, the HIX calculation is not identical in different studies (Birdwell & Engel, 2010; Inamdar et al., 2011; Lee et al., 2018; Ohno, 2002). We choose to use the formula after inner-filtering correction (Ohno, 2002) as our dataset spans a large range of DOC concentrations. HIX does show a clear relationship with tDOC%, but notably, the river data do not fall on the same relationship extrapolated from the coastal water data. It is well known that humic substances can be broken down after tDOC experiences biogeochemical processes, reducing the humification level (Catalán et al., 2013; Hansen et al., 2016; Huguet et al., 2009; Wilske et al., 2020). Nevertheless, some studies also report that DOM can be transformed to humified materials under photo-exposure or during microbial degradation, thus causing HIX to increase (Chen & Jaffé,

2014; Garcia et al., 2018; Hansen et al., 2016; Kieber et al., 1997; Ortega-Retuerta et al., 2010). The complex changing patterns during biogeochemical processes may make HIX insensitive above a certain level of humification or tDOC%. For example, we note that HIX showed almost no change during photo-exposure of the Maludam River samples (Figure 6g).

We additionally consider C2-Fmax/DOC, as it was used previously to estimate tDOC% for the Sarawak data, assuming that there would be no preferential removal of C2 relative to bulk tDOC over the small spatial scales of the estuaries in Sarawak (Zhou et al., 2019). Our new data from Singapore correspond to a longer water residence time, providing more opportunity for preferential removal of C2, which is expected to be fairly photo-labile (Grunert et al., 2021; Sankar et al., 2019). Some other studies have investigated relationships between absolute Fmax values and tDOC tracers such as lignin phenols (Osburn & Stedmon, 2011; Walker et al., 2013; Yang & Hur, 2014). However, given the substantial physical dilution, DOC normalization is appropriate. C2-Fmax/DOC is thus analogous to $SUVA_{254}$. Our data confirm that this measure is able to quantify tDOC% nearly as well as $SUVA_{254}$ across the large range seen in our Singapore Strait data, with a strong correlation coefficient (r^2=0.64, Figure 5i). This agrees with the strong linear correlation of C2 fluorescence to concentrations of lignin phenols obtained from Arctic rivers (Walker et al., 2013).

In contrast to these optical measures associated with tDOC, neither $S_{320–412}$ nor BIX were related to tDOC%, and indeed showed little variation throughout our time series. The Singapore Strait does not appear to experience large seasonality in phytoplankton production (Martin et al., 2022), and the production and microbial processing of autochthonous DOC are likely closely coupled year-round, with a relatively refractory marine DOC pool (Zhou et al., 2021). While our data thus cannot evaluate how well these two optical properties can trace the presence of freshly produced autochthonous DOC, our results do show that in the absence of fresh autochthonous DOC inputs, they show fairly stable values even as the DOC pool receives highly variable amounts of additional tDOC input (Figure 1f and Figure 2e).

Overall, our data thus demonstrate that all optical properties that are typically associated with tDOC (a_{440}, $S_{275–295}$, S_R, $SUVA_{254}$, FI, HIX and C2-Fmax/DOC) are indeed quantitatively related to tDOC% in coastal water, even after the tDOC has undergone a substantial degree of remineralization. However, the optical properties differ in the shape of the relationship to tDOC%,

718 indicating differences in applicability. $S_{275–295}$, S_R and HIX show non-linear change with tDOC%,
719 which makes them very sensitive to small changes in tDOC concentration at low tDOC%, but
720 much less sensitive to tDOC% above a certain level (~40%–60%). On the other hand, a_{440},
721 $SUVA_{254}$, FI and C2-Fmax/DOC present linear behaviors. This means that they are less sensitive
722 than the non-linear-related indicators at low tDOC%, but they show a consistent ability to quantify
723 tDOC% at least within the range of 0–60%. Clearly, however, the preferential removal of CDOM
724 means that a_λ needs to be used cautiously for quantifying tDOC if the range in possible
725 remineralization extent is large. The fact that $SUVA_{254}$ and C2-Fmax/DOC are normalized to DOC
726 concentration appears to make these measures more robust, although the need for DOC
727 measurements makes these parameters less easy and less rapid to measure. Thus, it is essential to
728 understand basic characteristics of certain water samples and consider measurement limitations
729 before choosing appropriate optical indicators to quantify tDOC%.

730 4.4 Qualitative proxies of tDOC biogeochemical processes

731 Our carbon stable isotope mass balance shows clearly that a variable proportion of the original
732 tDOC was remineralized before reaching our site. It has previously been demonstrated that
733 biodegradation and UV irradiation can cause optical properties to change in different directions
734 and/or at different rates (Hansen et al., 2016; Helms et al., 2008; Lee et al., 2018). Subsequently,
735 such changes might allow one to use optical properties to diagnose certain biogeochemical
736 processes: for example, photochemical and microbial degradation of tDOC are reported to affect
737 S_R differently (Hansen et al., 2016; Helms et al., 2008), while photochemical degradation
738 consistently increases $S_{275–295}$ (Fichot & Benner, 2012; Helms et al., 2014; Zhou et al., 2021). Here,
739 we additionally tested whether the optical properties can also be used to infer the extent of natural
740 tDOC remineralization in the environment. However, unlike the strong relationships to tDOC%,
741 and despite spanning a range of 20−80% tDOC loss, none of the optical properties showed any
742 consistent trends with tDOC loss (Figure S4).

743 The fact that the optical properties show little change with tDOC loss could arise from the
744 complexity of biogeochemical processes in the environment, where photodegradation,
745 biodegradation, and their interactions take place simultaneously (Del Vecchio & Blough, 2002;
746 Fovet et al., 2020; Lønborg et al., 2010; Osburn et al., 2009; Ward et al., 2017). Generally,
747 photodegradation is considered to play a significant role in tDOC remineralization. Yet, the extent

and rate of photo-induced remineralization and optical property change can vary depending on light intensities, irradiation wavelengths and specific origins of tDOC (Clark et al., 2020; Du et al., 2016; Hansen et al., 2016; Lee et al., 2018; Moran et al., 2000). It has been shown that biodegradation may cause optical properties of DOM to change less and possibly in an opposite direction compared to photodegradation (Hansen et al., 2016; Hernes & Benner, 2003; Hur et al., 2011; Lee et al., 2018). Microbial remineralization of tDOC is often significantly enhanced after partial photodegradation (Hansen et al., 2016; Miller & Moran, 1997; Moran et al., 2000), but conversely, photochemical reactions can also compete with microbial processes (Amado et al., 2015; Ward et al., 2017). In natural coastal environments, photo-induced reactions and microbial remineralization most likely always co-occur and interact at least to some degree. It is therefore possible that different co-occurring remineralization processes result in more limited changes in optical properties than those observed in single-process incubation experiments. A recent experimental study showed that microbial and combined photochemical + microbial degradation caused the optical properties of different plant leachates to converge over time despite large differences in initial properties (Harfmann et al., 2019). Tropical peatland tDOM experiences partial degradation within the peat dome before entering rivers (Gandois et al., 2014), so it is possible that the optical properties of the riverine tDOM pool have already undergone "microbial buffering" (Harfmann et al., 2019). Subsequent interactive photochemical and microbial degradation might then only have a limited impact on CDOM and FDOM spectral characteristics, consistent with our observations.

In the case of riverine tDOC from Southeast Asian peatlands, pure microbial remineralization appears to be relatively slow and no clear alteration of optical properties was found in microbial incubation experiments of 3–6 months duration (Nichols & Martin, 2021; Zhou et al., 2021). We therefore compare our environmental data to results from pure photodegradation experiments. For most parameters, especially $S_{275–295}$, S_R, and $SUVA_{254}$, we observed clear changes with consistent direction (i.e., increasing or decreasing) as a function of tDOC loss for both the peatland-draining river samples and the coastal water samples, and these changes are consistent with those reported previously for tDOM photobleaching experiments (Du et al., 2016; Helms et al., 2013; Lee et al., 2018; Magyan & Dempsey, 2021). Notably, we observed that the coastal water samples mostly showed much more obvious changes in optical properties for a given %tDOC loss than the river samples. The different rates of change are to be expected because coastal water samples contain

overall less CDOM and FDOM, and consist of a mixture of marine and terrestrial DOM, while the river samples still consisted of tDOM even at the end of the incubations. The results of bio- and photo-incubation for water from the peatland-draining river suggest that Southeast Asian peatland-derived tDOM behaves similar to other highly humified photo-labile but bio-refractory tDOM during remineralization (Chen & Jaffé, 2014; Dempsey et al., 2020). The fact that our environmental data do not demonstrate such clear relationships between optical properties and tDOC loss therefore suggests that natural tDOC remineralization in this region proceeds through complex interactive degradation processes that do not leave clear signatures in the optical properties. Further research would be valuable to understand how sequential and simultaneous photo- and biodegradation of tDOM alter its optical properties, which can help to further our interpretation of optical properties from natural water samples containing DOM from different sources and after environmental processing.

5 Conclusions

In summary, our study shows that there is preferential removal of optically active tDOM relative to total tDOC, but that DOM optical properties are nevertheless robust and potentially quantitative indicators of tDOC% in coastal waters. The commonly used optical properties a_{440}, $S_{275–295}$, S_R, $SUVA_{254}$, FI, and HIX, as well as C2-Fmax/DOC, can all quantify tDOC% in coastal water, but their relationships with tDOC% exhibit different shapes, accuracies and applicable ranges. Specifically, CDOM spectral slope parameters are very sensitive to the presence of low levels of tDOC, but show little further change once tDOC exceeds ~40% of total DOC. In contrast, $SUVA_{254}$ and C2-Fmax/DOC show linear relationships with tDOC contribution across a larger range of values. However, none of the optical properties we considered showed a relationship to the extent of tDOC remineralization, which we attribute to the likely complexity of multiple interacting biogeochemical degradation processes.

Acknowledgments

We thank Oon Yee Woo, Su Ping Heng, Kristy Y.W. Chang, Ashleen S.Y. Tan, Molly A. Moynihan, Robert S. Nichols, and Nikita Kaushal for help with field sampling and laboratory analysis, and the captains and crew of *Dolphin Explorer* and R/V *Galaxea* for support in the field. We are grateful to Richard Sanders for comments that helped to guide the analysis. This research was funded by the Singapore Ministry of Education through Academic Research Fund Tier 2 grant

MOE-MOET2EP10121-0007 and by the National Research Foundation, Singapore, Prime Minister's Office through grants MSRDP-P32 and NRF-NRI-2020-MESN.

Open Research

Processed data are available in the Supporting Information Data Set S1. The data that support the findings of this study are openly available in Nanyang Technological University Data Repository at https://doi.org/10.21979/N9/Q1L9HR.

References

Aksnes, D. L., Dupont, N., Staby, A., Fiksen, Ø., Kaartvedt, S., & Aure, J. (2009). Coastal water darkening and implications for mesopelagic regime shifts in Norwegian fjords. *Marine Ecology Progress Series*, *387*, 39-49. https://www.int-res.com/abstracts/meps/v387/p39-49/

Alling, V., Humborg, C., Mörth, C.-M., Rahm, L., & Pollehne, F. (2008). Tracing terrestrial organic matter by δ34S and δ13C signatures in a subarctic estuary. *53*(6), 2594-2602. https://doi.org/10.4319/lo.2008.53.6.2594

Alling, V., Porcelli, D., Mörth, C. M., Anderson, L. G., Sanchez-Garcia, L., Gustafsson, Ö., et al. (2012). Degradation of terrestrial organic carbon, primary production and out-gassing of CO2 in the Laptev and East Siberian Seas as inferred from δ13C values of DIC. *Geochimica et Cosmochimica Acta*, *95*, 143-159. https://doi.org/https://doi.org/10.1016/j.gca.2012.07.028

Amado, A. M., Cotner, J. B., Cory, R. M., Edhlund, B. L., & McNeill, K. (2015). Disentangling the Interactions Between Photochemical and Bacterial Degradation of Dissolved Organic Matter: Amino Acids Play a Central Role. *Microbial Ecology*, *69*(3), 554-566. https://doi.org/10.1007/s00248-014-0512-4

Anderson, T. R., Rowe, E. C., Polimene, L., Tipping, E., Evans, C. D., Barry, C. D. G., et al. (2019). Unified concepts for understanding and modelling turnover of dissolved organic matter from freshwaters to the ocean: the UniDOM model. *Biogeochemistry*, *146*(2), 105-123. https://doi.org/10.1007/s10533-019-00621-1

Antony, R., Willoughby, A. S., Grannas, A. M., Catanzano, V., Sleighter, R. L., Thamban, M., & Hatcher, P. G. (2018). Photo-biochemical transformation of dissolved organic matter on the surface of the coastal East Antarctic ice sheet. *Biogeochemistry*, *141*(2), 229-247. https://doi.org/10.1007/s10533-018-0516-0

Asmala, E., Stedmon, C. A., & Thomas, D. N. (2012). Linking CDOM spectral absorption to dissolved organic carbon concentrations and loadings in boreal estuaries. *Estuarine, Coastal and Shelf Science*, *111*, 107-117. https://doi.org/https://doi.org/10.1016/j.ecss.2012.06.015

Bauer, J. E. (2002). Chapter 8 - Carbon Isotopic Composition of DOM. In D. A. Hansell & C. A. Carlson (Eds.), *Biogeochemistry of marine dissolved organic matter* (pp. 405-453). Academic Press. https://doi.org/https://doi.org/10.1016/B978-012323841-2/50010-5

Bauer, J. E., & Bianchi, T. S. (2011). 5.02 - Dissolved Organic Carbon Cycling and Transformation. In E. Wolanski & D. McLusky (Eds.), *Treatise on Estuarine and Coastal Science* (pp. 7-67). Academic Press. https://doi.org/https://doi.org/10.1016/B978-0-12-374711-2.00502-7

Baum, A., Rixen, T., & Samiaji, J. (2007). Relevance of peat draining rivers in central Sumatra for the riverine input of dissolved organic carbon into the ocean. *Estuarine, Coastal and Shelf Science*, *73*(3), 563-570. https://doi.org/https://doi.org/10.1016/j.ecss.2007.02.012

Beaupré, S. R. (2015). Chapter 6 - The Carbon Isotopic Composition of Marine DOC. In D. A. Hansell & C. A. Carlson (Eds.), *Biogeochemistry of Marine Dissolved Organic Matter (Second Edition)* (pp. 335-368). Academic Press. https://doi.org/https://doi.org/10.1016/B978-0-12-405940-5.00006-6

Bélanger, S., Xie, H., Krotkov, N., Larouche, P., Vincent, W. F., & Babin, M. (2006). Photomineralization of terrigenous dissolved organic matter in Arctic coastal waters from 1979 to 2003: Interannual variability and implications of climate change. *Global Biogeochemical Cycles*, *20*(4). https://doi.org/https://doi.org/10.1029/2006GB002708

Beleites, C., & Sergo, V. (2018). hyperSpec: a package to handle hyperspectral data sets in R. *R package version 0.99-20180627, URL http://hyperspec. r-forge. r-project. org*.

Benner, R., & Kaiser, K. (2011). Biological and photochemical transformations of amino acids and lignin phenols in riverine dissolved organic matter. *Biogeochemistry*, *102*(1), 209-222. https://doi.org/10.1007/s10533-010-9435-4

Benner, R., Louchouarn, P., & Amon, R. M. W. (2005). Terrigenous dissolved organic matter in the Arctic Ocean and its transport to surface and deep waters of the North Atlantic. *Global Biogeochemical Cycles*, *19*(2). https://doi.org/https://doi.org/10.1029/2004GB002398

Berggren, M., Guillemette, F., Bieroza, M., Buffam, I., Deininger, A., Hawkes, J. A., et al. (2022). Unified understanding of intrinsic and extrinsic controls of dissolved organic carbon reactivity in aquatic ecosystems. *Ecology*, *103*(9), e3763. https://doi.org/https://doi.org/10.1002/ecy.3763

Birdwell, J. E., & Engel, A. S. (2010). Characterization of dissolved organic matter in cave and spring waters using UV–Vis absorbance and fluorescence spectroscopy. *Organic Geochemistry*, *41*(3), 270-280. https://doi.org/https://doi.org/10.1016/j.orggeochem.2009.11.002

Cao, X., Aiken, G. R., Butler, K. D., Huntington, T. G., Balch, W. M., Mao, J., & Schmidt-Rohr, K. (2018). Evidence for major input of riverine organic matter into the ocean. *Organic Geochemistry*, *116*, 62-76. https://doi.org/https://doi.org/10.1016/j.orggeochem.2017.11.001

Capelle, D. W., Kuzyk, Z. Z. A., Papakyriakou, T., Guéguen, C., Miller, L. A., & Macdonald, R. W. (2020). Effect of terrestrial organic matter on ocean acidification and CO2 flux in an Arctic shelf sea. *Progress in Oceanography*, *185*, 102319. https://doi.org/https://doi.org/10.1016/j.pocean.2020.102319

Cartisano, C. M., Del Vecchio, R., Bianca, M. R., & Blough, N. V. (2018). Investigating the sources and structure of chromophoric dissolved organic matter (CDOM) in the North Pacific Ocean (NPO) utilizing optical spectroscopy combined with solid phase extraction and borohydride reduction. *Marine Chemistry*, *204*, 20-35. https://doi.org/https://doi.org/10.1016/j.marchem.2018.05.005

Catalán, N., Obrador, B., Felip, M., & Pretus, J. L. (2013). Higher reactivity of allochthonous vs. autochthonous DOC sources in a shallow lake. *Aquatic Sciences*, *75*(4), 581-593. https://doi.org/10.1007/s00027-013-0302-y

Chen, M., & Jaffé, R. (2014). Photo- and bio-reactivity patterns of dissolved organic matter from biomass and soil leachates and surface waters in a subtropical wetland. *Water Research*, *61*, 181-190. https://doi.org/https://doi.org/10.1016/j.watres.2014.03.075

Chen, Y., Liu, J., Zhang, X., & Blough, N. V. (2020). Time-Resolved Fluorescence Spectra of Untreated and Sodium Borohydride-Reduced Chromophoric Dissolved Organic Matter. *Environmental Science & Technology*, *54*(19), 12109-12118. https://doi.org/10.1021/acs.est.0c03135

Chen, Z., Doering, P. H., Ashton, M., & Orlando, B. A. (2015). Mixing behavior of colored dissolved organic matter and its potential ecological implication in the Caloosahatchee River Estuary, Florida. *Estuaries and Coasts*, *38*(5), 1706-1718. https://doi.org/10.1007/s12237-014-9916-0

Chin, Y.-P., Aiken, G., & O'Loughlin, E. (1994). Molecular weight, polydispersity, and spectroscopic properties of aquatic humic substances. *Environmental Science & Technology*, *28*(11), 1853-1858. https://doi.org/10.1021/es00060a015

Ciais, P., Sabine, C., Bala, G., & Peters, W. (2013). Carbon and Other Biogeochemical Cycles. In T. F. Stocker, D. Qin, G. K. Plattner, M. Tignor, S. K. Allen, J. Boschung, A. Nauels, Y. Xia, V. Bex, & P. M. Midgley (Eds.), *Climate Change 2013: The Physical Science Basis. Contribution of Working Group I to the Fifth Assessment Report of the Intergovernmental Panel on Climate Change* (pp. 465-570). Cambridge University Press. https://edepot.wur.nl/345905

Clark, C. D., De Bruyn, W. J., Brahm, B., & Aiona, P. (2020). Optical properties of chromophoric dissolved organic matter (CDOM) and dissolved organic carbon (DOC) levels in constructed water treatment wetland systems in southern California, USA. *Chemosphere*, *247*, 125906. https://doi.org/https://doi.org/10.1016/j.chemosphere.2020.125906

Coble, P. G. (1996). Characterization of marine and terrestrial DOM in seawater using excitation-emission matrix spectroscopy. *Marine Chemistry*, *51*(4), 325-346. https://doi.org/https://doi.org/10.1016/0304-4203(95)00062-3

Coble, P. G. (2007). Marine Optical Biogeochemistry: The Chemistry of Ocean Color. *Chemical Reviews*, *107*(2), 402-418. https://doi.org/10.1021/cr050350+

Cory, R. M., & Kling, G. W. (2018). Interactions between sunlight and microorganisms influence dissolved organic matter degradation along the aquatic continuum. *Limnology and Oceanography Letters*, *3*(3), 102-116. https://doi.org/10.1002/lol2.10060

Cory, R. M., & McKnight, D. M. (2005). Fluorescence spectroscopy reveals ubiquitous presence of oxidized and reduced quinones in dissolved organic matter. *Environmental Science & Technology*, *39*(21), 8142-8149. https://doi.org/10.1021/es0506962

Cory, R. M., Miller, M. P., McKnight, D. M., Guerard, J. J., & Miller, P. L. (2010). Effect of instrument-specific response on the analysis of fulvic acid fluorescence spectra. *Limnology and Oceanography: Methods*, *8*(2), 67-78. https://doi.org/https://doi.org/10.4319/lom.2010.8.67

Dai, M., Yin, Z., Meng, F., Liu, Q., & Cai, W.-J. (2012). Spatial distribution of riverine DOC inputs to the ocean: an updated global synthesis. *Current Opinion in Environmental Sustainability*, *4*(2), 170-178. https://doi.org/https://doi.org/10.1016/j.cosust.2012.03.003

Danhiez, F. P., Vantrepotte, V., Cauvin, A., Lebourg, E., & Loisel, H. (2017). Optical properties of chromophoric dissolved organic matter during a phytoplankton bloom. Implication for DOC estimates from CDOM absorption. *Limnology and Oceanography*, *62*(4), 1409-1425. https://doi.org/https://doi.org/10.1002/lno.10507

Del Vecchio, R., & Blough, N. V. (2002). Photobleaching of chromophoric dissolved organic matter in natural waters: kinetics and modeling. *Marine Chemistry*, *78*(4), 231-253. https://doi.org/https://doi.org/10.1016/S0304-4203(02)00036-1

Del Vecchio, R., & Blough, N. V. (2004a). On the Origin of the Optical Properties of Humic Substances. *Environmental Science & Technology*, *38*(14), 3885-3891. https://doi.org/10.1021/es049912h

Del Vecchio, R., & Blough, N. V. (2004b). Spatial and seasonal distribution of chromophoric dissolved organic matter and dissolved organic carbon in the Middle Atlantic Bight. *Marine Chemistry*, *89*(1), 169-187. https://doi.org/https://doi.org/10.1016/j.marchem.2004.02.027

Dempsey, C. M., Brentrup, J. A., Magyan, S., Knoll, L. B., Swain, H. M., Gaiser, E. E., et al. (2020). The relative importance of photodegradation and biodegradation of terrestrially derived dissolved organic carbon across four lakes of differing trophic status. *Biogeosciences*, *17*(24), 6327-6340. https://doi.org/10.5194/bg-17-6327-2020

Dittmar, T. (2015). Chapter 7 - Reasons Behind the Long-Term Stability of Dissolved Organic Matter. In D. A. Hansell & C. A. Carlson (Eds.), *Biogeochemistry of Marine Dissolved Organic Matter (Second Edition)* (pp. 369-388). Academic Press. https://doi.org/https://doi.org/10.1016/B978-0-12-405940-5.00007-8

Du, Y., Zhang, Y., Chen, F., Chang, Y., & Liu, Z. (2016). Photochemical reactivities of dissolved organic matter (DOM) in a sub-alpine lake revealed by EEM-PARAFAC: An insight into the fate of allochthonous DOM in alpine lakes affected by climate change. *Science of The Total Environment*, *568*, 216-225. https://doi.org/https://doi.org/10.1016/j.scitotenv.2016.06.036

Evans, C. D., Page, S. E., Jones, T., Moore, S., Gauci, V., Laiho, R., et al. (2014). Contrasting vulnerability of drained tropical and high-latitude peatlands to fluvial loss of stored carbon. *Global Biogeochemical Cycles*, *28*(11), 1215-1234. https://doi.org/https://doi.org/10.1002/2013GB004782

Fichot, C. G., & Benner, R. (2011). A novel method to estimate DOC concentrations from CDOM absorption coefficients in coastal waters. *Geophysical Research Letters*, *38*(3), n/a-n/a. https://doi.org/10.1029/2010gl046152

Fichot, C. G., & Benner, R. (2012). The spectral slope coefficient of chromophoric dissolved organic matter (S275–295) as a tracer of terrigenous dissolved organic carbon in river-influenced ocean margins. *Limnology and Oceanography*, *57*(5), 1453-1466. https://doi.org/10.4319/lo.2012.57.5.1453

Fichot, C. G., & Benner, R. (2014). The fate of terrigenous dissolved organic carbon in a river-influenced ocean margin. *Global Biogeochemical Cycles*, *28*(3), 300-318. https://doi.org/https://doi.org/10.1002/2013GB004670

Fichot, C. G., Benner, R., Kaiser, K., Shen, Y., Amon, R. M. W., Ogawa, H., & Lu, C.-J. (2016). Predicting Dissolved Lignin Phenol Concentrations in the Coastal Ocean from Chromophoric Dissolved Organic Matter (CDOM) Absorption Coefficients [Original Research]. *Frontiers in Marine Science*, *3*(7). https://doi.org/10.3389/fmars.2016.00007

Fovet, O., Cooper, D. M., Jones, D. L., Jones, T. G., & Evans, C. D. (2020). Dynamics of dissolved organic matter in headwaters: comparison of headwater streams with contrasting DOM and nutrient composition. *Aquatic Sciences*, *82*(2), 29. https://doi.org/10.1007/s00027-020-0704-6

Gandois, L., Teisserenc, R., Cobb, A. R., Chieng, H. I., Lim, L. B. L., Kamariah, A. S., et al. (2014). Origin, composition, and transformation of dissolved organic matter in tropical peatlands. *Geochimica et Cosmochimica Acta*, *137*, 35-47. https://doi.org/https://doi.org/10.1016/j.gca.2014.03.012

Garcia, R. D., Diéguez, M. d. C., Gerea, M., Garcia, P. E., & Reissig, M. (2018). Characterisation and reactivity continuum of dissolved organic matter in forested headwater catchments of Andean Patagonia. *Freshwater Biology*, *63*(9), 1049-1062. https://doi.org/https://doi.org/10.1111/fwb.13114

Gran, G. (1952). Determination of the equivalence point in potentiometric titrations. Part II. *The Analyst*, *77*(920), 661. https://doi.org/10.1039/an9527700661

968 Green, S. A., & Blough, N. V. (1994). Optical absorption and fluorescence properties of chromophoric dissolved
969 organic matter in natural waters. *Limnology and Oceanography*, *39*(8), 1903-1916.
970 https://doi.org/https://doi.org/10.4319/lo.1994.39.8.1903
971 Grunert, B. K., Tzortziou, M., Neale, P., Menendez, A., & Hernes, P. (2021). DOM degradation by light and microbes
972 along the Yukon River-coastal ocean continuum. *Scientific Reports*, *11*(1), 10236.
973 https://doi.org/10.1038/s41598-021-89327-9
974 Hansen, A. M., Kraus, T. E. C., Pellerin, B. A., Fleck, J. A., Downing, B. D., & Bergamaschi, B. A. (2016). Optical
975 properties of dissolved organic matter (DOM): Effects of biological and photolytic degradation. *Limnology*
976 *and Oceanography*, *61*(3), 1015-1032. https://doi.org/10.1002/lno.10270
977 Harfmann, J. L., Guillemette, F., Kaiser, K., Spencer, R. G. M., Chuang, C.-Y., & Hernes, P. J. (2019). Convergence
978 of Terrestrial Dissolved Organic Matter Composition and the Role of Microbial Buffering in Aquatic
979 Ecosystems. *Journal of Geophysical Research: Biogeosciences*, *124*(10), 3125-3142.
980 https://doi.org/https://doi.org/10.1029/2018JG004997
981 Harun, S., Baker, A., Bradley, C., & Pinay, G. (2016). Spatial and seasonal variations in the composition of dissolved
982 organic matter in a tropical catchment: the Lower Kinabatangan River, Sabah, Malaysia
983 [10.1039/C5EM00462D]. *Environmental Science: Processes & Impacts*, *18*(1), 137-150.
984 https://doi.org/10.1039/C5EM00462D
985 Hedges, J. I., Keil, R. G., & Benner, R. (1997). What happens to terrestrial organic matter in the ocean? *Organic*
986 *Geochemistry*, *27*(5), 195-212. https://doi.org/https://doi.org/10.1016/S0146-6380(97)00066-1
987 Helms, J. R., Mao, J., Stubbins, A., Schmidt-Rohr, K., Spencer, R. G. M., Hernes, P. J., & Mopper, K. (2014). Loss
988 of optical and molecular indicators of terrigenous dissolved organic matter during long-term photobleaching.
989 *Aquatic Sciences*, *76*(3), 353-373. https://doi.org/10.1007/s00027-014-0340-0
990 Helms, J. R., Stubbins, A., Perdue, E. M., Green, N. W., Chen, H., & Mopper, K. (2013). Photochemical bleaching of
991 oceanic dissolved organic matter and its effect on absorption spectral slope and fluorescence. *Marine*
992 *Chemistry*, *155*, 81-91. https://doi.org/https://doi.org/10.1016/j.marchem.2013.05.015
993 Helms, J. R., Stubbins, A., Ritchie, J. D., Minor, E. C., Kieber, D. J., & Mopper, K. (2008). Absorption spectral slopes
994 and slope ratios as indicators of molecular weight, source, and photobleaching of chromophoric dissolved
995 organic matter. *Limnology and Oceanography*, *53*(3), 955-969. https://doi.org/10.4319/lo.2008.53.3.0955
996 Hernes, P. J., & Benner, R. (2003). Photochemical and microbial degradation of dissolved lignin phenols: Implications
997 for the fate of terrigenous dissolved organic matter in marine environments. *Journal of Geophysical*
998 *Research: Oceans*, *108*(C9). https://doi.org/10.1029/2002jc001421
999 Huang, T. H., Chen, C. T. A., Tseng, H. C., Lou, J. Y., Wang, S. L., Yang, L., et al. (2017). Riverine carbon fluxes to
1000 the South China Sea. *Journal of Geophysical Research: Biogeosciences*, *122*(5), 1239-1259.
1001 https://doi.org/https://doi.org/10.1002/2016JG003701
1002 Huguet, A., Vacher, L., Relexans, S., Saubusse, S., Froidefond, J. M., & Parlanti, E. (2009). Properties of fluorescent
1003 dissolved organic matter in the Gironde Estuary. *Organic Geochemistry*, *40*(6), 706-719.
1004 https://doi.org/https://doi.org/10.1016/j.orggeochem.2009.03.002
1005 Humborg, C., Geibel, M. C., Anderson, L. G., Björk, G., Mörth, C.-M., Sundbom, M., et al. (2017). Sea-air exchange
1006 patterns along the central and outer East Siberian Arctic Shelf as inferred from continuous CO2, stable
1007 isotope, and bulk chemistry measurements. *Global Biogeochemical Cycles*, *31*(7), 1173-1191.
1008 https://doi.org/https://doi.org/10.1002/2017GB005656
1009 Hur, J., Jung, K.-Y., & Schlautman, M. A. (2011). Altering the characteristics of a leaf litter-derived humic substance
1010 by adsorptive fractionation versus simulated solar irradiation. *Water Research*, *45*(18), 6217-6226.
1011 https://doi.org/https://doi.org/10.1016/j.watres.2011.09.023
1012 Hur, J., Williams, M. A., & Schlautman, M. A. (2006). Evaluating spectroscopic and chromatographic techniques to
1013 resolve dissolved organic matter via end member mixing analysis. *Chemosphere*, *63*(3), 387-402.
1014 https://doi.org/https://doi.org/10.1016/j.chemosphere.2005.08.069
1015 Inamdar, S., Singh, S., Dutta, S., Levia, D., Mitchell, M., Scott, D., et al. (2011). Fluorescence characteristics and
1016 sources of dissolved organic matter for stream water during storm events in a forested mid-Atlantic
1017 watershed. *Journal of Geophysical Research: Biogeosciences*, *116*(G3).
1018 https://doi.org/https://doi.org/10.1029/2011JG001735
1019 Jaffé, R., Cawley, K. M., & Yamashita, Y. (2014). Applications of Excitation Emission Matrix Fluorescence with
1020 Parallel Factor Analysis (EEM-PARAFAC) in Assessing Environmental Dynamics of Natural Dissolved
1021 Organic Matter (DOM) in Aquatic Environments: A Review. In *Advances in the Physicochemical*
1022 *Characterization of Dissolved Organic Matter: Impact on Natural and Engineered Systems* (Vol. 1160, pp.
1023 27-73). American Chemical Society. https://doi.org/doi:10.1021/bk-2014-1160.ch003

10.1021/bk-2014-1160.ch003
Kaiser, K., Benner, R., & Amon, R. M. W. (2017). The fate of terrigenous dissolved organic carbon on the Eurasian shelves and export to the North Atlantic. *Journal of Geophysical Research: Oceans*, *122*(1), 4-22. https://doi.org/https://doi.org/10.1002/2016JC012380
Kang, P.-G., & Mitchell, M. J. (2013). Bioavailability and size-fraction of dissolved organic carbon, nitrogen, and sulfur at the Arbutus Lake watershed, Adirondack Mountains, NY. *Biogeochemistry*, *115*(1), 213-234. https://doi.org/10.1007/s10533-013-9829-1
Karen, L. B.-N., & Mary Ann, M. (1999). Photochemical formation of biologically available nitrogen from dissolved humic substances in coastal marine systems. *Aquatic Microbial Ecology*, *18*(3), 285-292. https://www.int-res.com/abstracts/ame/v18/n3/p285-292/
Kartadikaria, A. R., Watanabe, A., Nadaoka, K., Adi, N. S., Prayitno, H. B., Soemorumekso, S., et al. (2015). CO2 sink/source characteristics in the tropical Indonesian seas. *Journal of Geophysical Research: Oceans*, *120*(12), 7842-7856. https://doi.org/https://doi.org/10.1002/2015JC010925
Kida, M., Fujitake, N., Suchewaboripont, V., Poungparn, S., Tomotsune, M., Kondo, M., et al. (2018). Contribution of humic substances to dissolved organic matter optical properties and iron mobilization. *Aquatic Sciences*, *80*(3), 26. https://doi.org/10.1007/s00027-018-0578-z
Kieber, R. J., Hydro, L. H., & Seaton, P. J. (1997). Photooxidation of triglycerides and fatty acids in seawater: Implication toward the formation of marine humic substances. *Limnology and Oceanography*, *42*(6), 1454-1462. https://doi.org/https://doi.org/10.4319/lo.1997.42.6.1454
Kowalczuk, P., Tilstone, G. H., Zabłocka, M., Röttgers, R., & Thomas, R. (2013). Composition of dissolved organic matter along an Atlantic Meridional Transect from fluorescence spectroscopy and Parallel Factor Analysis. *Marine Chemistry*, *157*, 170-184. https://doi.org/https://doi.org/10.1016/j.marchem.2013.10.004
Lawaetz, A. J., & Stedmon, C. A. (2009). Fluorescence Intensity Calibration Using the Raman Scatter Peak of Water. *Applied Spectroscopy*, *63*(8), 936-940. https://doi.org/10.1366/000370209788964548
Lee, M.-H., Osburn, C. L., Shin, K.-H., & Hur, J. (2018). New insight into the applicability of spectroscopic indices for dissolved organic matter (DOM) source discrimination in aquatic systems affected by biogeochemical processes. *Water Research*, *147*, 164-176. https://doi.org/https://doi.org/10.1016/j.watres.2018.09.048
Lee, S. A., Kim, T. H., & Kim, G. (2020). Tracing terrestrial versus marine sources of dissolved organic carbon in a coastal bay using stable carbon isotopes. *Biogeosciences*, *17*(1), 135-144. https://doi.org/10.5194/bg-17-135-2020
Letscher, R. T., Hansell, D. A., & Kadko, D. (2011). Rapid removal of terrigenous dissolved organic carbon over the Eurasian shelves of the Arctic Ocean. *Marine Chemistry*, *123*(1), 78-87. https://doi.org/https://doi.org/10.1016/j.marchem.2010.10.002
Lønborg, C., Álvarez-Salgado, X. A., Davidson, K., Martínez-García, S., & Teira, E. (2010). Assessing the microbial bioavailability and degradation rate constants of dissolved organic matter by fluorescence spectroscopy in the coastal upwelling system of the Ría de Vigo. *Marine Chemistry*, *119*(1), 121-129. https://doi.org/https://doi.org/10.1016/j.marchem.2010.02.001
Louchouarn, P., Opsahl, S., & Benner, R. (2000). Isolation and Quantification of Dissolved Lignin from Natural Waters Using Solid-Phase Extraction and GC/MS. *Analytical Chemistry*, *72*(13), 2780-2787. https://doi.org/10.1021/ac9912552
Lu, C.-J., Benner, R., Fichot, C. G., Fukuda, H., Yamashita, Y., & Ogawa, H. (2016). Sources and Transformations of Dissolved Lignin Phenols and Chromophoric Dissolved Organic Matter in Otsuchi Bay, Japan [Original Research]. *Frontiers in Marine Science*, *3*(85). https://doi.org/10.3389/fmars.2016.00085
Magyan, S., & Dempsey, C. M. (2021). The role of time and mixing in the degradation of terrestrial derived dissolved organic carbon in lakes of varying trophic status. *Journal of Photochemistry and Photobiology*, *8*, 100065. https://doi.org/https://doi.org/10.1016/j.jpap.2021.100065
Mann, P. J., Spencer, R. G. M., Hernes, P. J., Six, J., Aiken, G. R., Tank, S. E., et al. (2016). Pan-Arctic Trends in Terrestrial Dissolved Organic Matter from Optical Measurements [Original Research]. *4*(25). https://doi.org/10.3389/feart.2016.00025
Martin, P., Cherukuru, N., Tan, A. S. Y., Sanwlani, N., Mujahid, A., & Müller, M. (2018). Distribution and cycling of terrigenous dissolved organic carbon in peatland-draining rivers and coastal waters of Sarawak, Borneo. *Biogeosciences*, *15*(22), 6847-6865. https://doi.org/10.5194/bg-15-6847-2018
Martin, P., Moynihan, M. A., Chen, S., Woo, O. Y., Zhou, Y., Nichols, R. S., et al. (2022). Monsoon-driven biogeochemical dynamics in an equatorial shelf sea: Time-series observations in the Singapore Strait. *Estuarine, Coastal and Shelf Science*, *270*, 107855. https://doi.org/https://doi.org/10.1016/j.ecss.2022.107855

Martin, P., Sanwlani, N., Lee, T. W. Q., Wong, J. M. C., Chang, K. Y. W., Wong, E. W. S., & Liew, S. C. (2021). Dissolved organic matter from tropical peatlands reduces shelf sea light availability in the Singapore Strait, Southeast Asia. *Marine Ecology Progress Series*, *672*, 89-109. https://www.int-res.com/abstracts/meps/v672/p89-109/

Massicotte, P., Asmala, E., Stedmon, C., & Markager, S. (2017). Global distribution of dissolved organic matter along the aquatic continuum: Across rivers, lakes and oceans. *Science of The Total Environment*, *609*, 180-191. https://doi.org/https://doi.org/10.1016/j.scitotenv.2017.07.076

Mayer, B., & Pohlmann, T. (2014). Simulation of organic pollutants: First step towards an adaptation to the Malacca Strait. *Asian Journal of Water, Environment and Pollution*, *11*, 75-86.

Mayer, B., Siegel, H., Gerth, M., Pohlmann, T., Stottmeister, I., Putri, M., & Setiawan, A. (2022). 2 - Physical environment of the Indonesian Seas with focus on the western region. In T. C. Jennerjahn, T. Rixen, H. E. Irianto, & J. Samiaji (Eds.), *Science for the Protection of Indonesian Coastal Ecosystems (SPICE)* (pp. 13-43). Elsevier. https://doi.org/https://doi.org/10.1016/B978-0-12-815050-4.00007-9

McKnight, D. M., Boyer, E. W., Westerhoff, P. K., Doran, P. T., Kulbe, T., & Andersen, D. T. (2001). Spectrofluorometric characterization of dissolved organic matter for indication of precursor organic material and aromaticity. *Limnology and Oceanography*, *46*(1), 38-48. https://doi.org/10.4319/lo.2001.46.1.0038

Medeiros, P. M., Seidel, M., Niggemann, J., Spencer, R. G. M., Hernes, P. J., Yager, P. L., et al. (2016). A novel molecular approach for tracing terrigenous dissolved organic matter into the deep ocean. *Global Biogeochemical Cycles*, *30*(5), 689-699. https://doi.org/https://doi.org/10.1002/2015GB005320

Meyers-Schulte, K. J., & Hedges, J. I. (1986). Molecular evidence for a terrestrial component of organic matter dissolved in ocean water. *Nature*, *321*(6065), 61-63. https://doi.org/10.1038/321061a0

Miller, W. L., & Moran, M. A. (1997). Interaction of photochemical and microbial processes in the degradation of refractory dissolved organic matter from a coastal marine environment. *Limnology and Oceanography*, *42*(6), 1317-1324. https://doi.org/https://doi.org/10.4319/lo.1997.42.6.1317

Mizubayashi, K., Kuwahara, V. S., Segaran, T. C., Zaleha, K., Effendy, A. W. M., Kushairi, M. R. M., & Toda, T. (2013). Monsoon variability of ultraviolet radiation (UVR) attenuation and bio-optical factors in the Asian tropical coral-reef waters. *Estuarine, Coastal and Shelf Science*, *126*, 34-43. https://doi.org/https://doi.org/10.1016/j.ecss.2013.04.002

Moore, S., Gauci, V., Evans, C. D., & Page, S. E. (2011). Fluvial organic carbon losses from a Bornean blackwater river. *Biogeosciences*, *8*(4), 901-909. https://doi.org/10.5194/bg-8-901-2011

Moran, M. A., Sheldon Jr., W. M., & Zepp, R. G. (2000). Carbon loss and optical property changes during long-term photochemical and biological degradation of estuarine dissolved organic matter. *Limnology and Oceanography*, *45*(6), 1254-1264. https://doi.org/https://doi.org/10.4319/lo.2000.45.6.1254

Morgan, K. M., Moynihan, M. A., Sanwlani, N., & Switzer, A. D. (2020). Light Limitation and Depth-Variable Sedimentation Drives Vertical Reef Compression on Turbid Coral Reefs [Original Research]. *Frontiers in Marine Science*, *7*. https://doi.org/10.3389/fmars.2020.571256

Müller, D., Warneke, T., Rixen, T., Müller, M., Jamahari, S., Denis, N., et al. (2015). Lateral carbon fluxes and CO₂ outgassing from a tropical peat-draining river. *Biogeosciences*, *12*(20), 5967-5979. https://doi.org/10.5194/bg-12-5967-2015

Murphy, K. R., Stedmon, C. A., Graeber, D., & Bro, R. (2013). Fluorescence spectroscopy and multi-way techniques. PARAFAC [10.1039/C3AY41160E]. *Analytical Methods*, *5*(23), 6557-6566. https://doi.org/10.1039/C3AY41160E

Murphy, K. R., Stedmon, C. A., Waite, T. D., & Ruiz, G. M. (2008). Distinguishing between terrestrial and autochthonous organic matter sources in marine environments using fluorescence spectroscopy. *Marine Chemistry*, *108*(1), 40-58. https://doi.org/https://doi.org/10.1016/j.marchem.2007.10.003

Nichols, R. S., & Martin, P. (2021). Low Biodegradability of Dissolved Organic Matter From Southeast Asian Peat-Draining Rivers. *Journal of Geophysical Research: Biogeosciences*, *126*(6), e2020JG006182. https://doi.org/https://doi.org/10.1029/2020JG006182

Ohno, T. (2002). Fluorescence Inner-Filtering Correction for Determining the Humification Index of Dissolved Organic Matter. *Environmental Science & Technology*, *36*(4), 742-746. https://doi.org/10.1021/es0155276

Opsahl, S., & Benner, R. (1997). Distribution and cycling of terrigenous dissolved organic matter in the ocean. *Nature*, *386*(6624), 480-482. https://doi.org/10.1038/386480a0

Opsahl, S., & Benner, R. (1998). Photochemical reactivity of dissolved lignin in river and ocean waters. *Limnology and Oceanography*, *43*(6), 1297-1304. https://doi.org/https://doi.org/10.4319/lo.1998.43.6.1297

1134 Opsahl, S. P., & Zepp, R. G. (2001). Photochemically-induced alteration of stable carbon isotope ratios (δ13C) in
1135 terrigenous dissolved organic carbon. *Geophysical Research Letters*, *28*(12), 2417-2420.
1136 https://doi.org/10.1029/2000gl012686
1137 Ortega-Retuerta, E., Reche, I., Pulido-Villena, E., Agustí, S., & Duarte, C. M. (2010). Distribution and photoreactivity
1138 of chromophoric dissolved organic matter in the Antarctic Peninsula (Southern Ocean). *Marine Chemistry*,
1139 *118*(3), 129-139. https://doi.org/https://doi.org/10.1016/j.marchem.2009.11.008
1140 Osburn, C. L., Boyd, T. J., Montgomery, M. T., Bianchi, T. S., Coffin, R. B., & Paerl, H. W. (2016). Optical proxies
1141 for terrestrial dissolved organic matter in estuaries and coastal Waters [Original Research]. *Frontiers in*
1142 *Marine Science*, *2*(127). https://doi.org/10.3389/fmars.2015.00127
1143 Osburn, C. L., Morris, D. P., Thorn, K. A., & Moeller, R. E. (2001). Chemical and optical changes in freshwater
1144 dissolved organic matter exposed to solar radiation. *Biogeochemistry*, *54*(3), 251-278.
1145 https://doi.org/10.1023/A:1010657428418
1146 Osburn, C. L., Retamal, L., & Vincent, W. F. (2009). Photoreactivity of chromophoric dissolved organic matter
1147 transported by the Mackenzie River to the Beaufort Sea. *Marine Chemistry*, *115*(1), 10-20.
1148 https://doi.org/https://doi.org/10.1016/j.marchem.2009.05.003
1149 Osburn, C. L., & Stedmon, C. A. (2011). Linking the chemical and optical properties of dissolved organic matter in
1150 the Baltic–North Sea transition zone to differentiate three allochthonous inputs. *Marine Chemistry*, *126*(1),
1151 281-294. https://doi.org/https://doi.org/10.1016/j.marchem.2011.06.007
1152 Painter, S. C., Lapworth, D. J., Woodward, E. M. S., Kroeger, S., Evans, C. D., Mayor, D. J., & Sanders, R. J. (2018).
1153 Terrestrial dissolved organic matter distribution in the North Sea. *Science of The Total Environment*, *630*,
1154 630-647. https://doi.org/https://doi.org/10.1016/j.scitotenv.2018.02.237
1155 Qualls, R. G., & Richardson, C. J. (2003). Factors controlling concentration, export, and decomposition of dissolved
1156 organic nutrients in the Everglades of Florida. *Biogeochemistry*, *62*(2), 197-229.
1157 https://doi.org/10.1023/A:1021150503664
1158 Raymond, P. A., & Spencer, R. G. M. (2015). Chapter 11 - Riverine DOM. In D. A. Hansell & C. A. Carlson (Eds.),
1159 *Biogeochemistry of Marine Dissolved Organic Matter (Second Edition)* (pp. 509-533). Academic Press.
1160 https://doi.org/https://doi.org/10.1016/B978-0-12-405940-5.00011-X
1161 Reader, H. E., & Miller, W. L. (2012). Variability of carbon monoxide and carbon dioxide apparent quantum yield
1162 spectra in three coastal estuaries of the South Atlantic Bight. *Biogeosciences*, *9*(11), 4279-4294.
1163 https://doi.org/10.5194/bg-9-4279-2012
1164 Rixen, T., Wit, F., Hutahaean, A. A., Schlüter, A., Baum, A., Klemme, A., et al. (2022). 4 - Carbon cycle in tropical
1165 peatlands and coastal seas. In T. C. Jennerjahn, T. Rixen, H. E. Irianto, & J. Samiaji (Eds.), *Science for the*
1166 *Protection of Indonesian Coastal Ecosystems (SPICE)* (pp. 83-142). Elsevier.
1167 https://doi.org/https://doi.org/10.1016/B978-0-12-815050-4.00011-0
1168 Ronald Benner, & Kaiser, K. (2011). Biological and photochemical transformations of amino acids and lignin phenols
1169 in riverine dissolved organic matter. *Biogeochemistry*, *102*(1-3), 209-222.
1170 https://doi.org/https://doi.org/10.1007/s10533-010-9435-4
1171 Samanta, S., Dalai, T. K., Pattanaik, J. K., Rai, S. K., & Mazumdar, A. (2015). Dissolved inorganic carbon (DIC) and
1172 its δ13C in the Ganga (Hooghly) River estuary, India: Evidence of DIC generation via organic carbon
1173 degradation and carbonate dissolution. *Geochimica et Cosmochimica Acta*, *165*, 226-248.
1174 https://doi.org/https://doi.org/10.1016/j.gca.2015.05.040
1175 Sankar, M. S., Dash, P., Singh, S., Lu, Y., Mercer, A. E., & Chen, S. (2019). Effect of photo-biodegradation and
1176 biodegradation on the biogeochemical cycling of dissolved organic matter across diverse surface water
1177 bodies. *Journal of Environmental Sciences*, *77*, 130-147.
1178 https://doi.org/https://doi.org/10.1016/j.jes.2018.06.021
1179 Santos, L., Pinto, A., Filipe, O., Cunha, Â., Santos, E. B. H., & Almeida, A. (2016). Insights on the Optical Properties
1180 of Estuarine DOM - Hydrological and Biological Influences. *PloS one*, *11*(5), e0154519-e0154519.
1181 https://doi.org/10.1371/journal.pone.0154519
1182 Schmitt-Kopplin, P., Hertkorn, N., Schulten, H.-R., & Kettrup, A. (1998). Structural Changes in a Dissolved Soil
1183 Humic Acid during Photochemical Degradation Processes under O2 and N2 Atmosphere. *Environmental*
1184 *Science & Technology*, *32*(17), 2531-2541. https://doi.org/10.1021/es970636z
1185 Semiletov, I., Pipko, I., Gustafsson, Ö., Anderson, L. G., Sergienko, V., Pugach, S., et al. (2016). Acidification of East
1186 Siberian Arctic Shelf waters through addition of freshwater and terrestrial carbon. *Nature Geoscience*, *9*(5),
1187 361-365. https://doi.org/10.1038/ngeo2695

1188 Siegel, H., Gerth, M., Stottmeister, I., Baum, A., & Samiaji, J. (2019). Remote sensing of coastal discharge of SE
1189 Sumatra (Indonesia). In V. Barale & M. Gade (Eds.), *Remote Sensing of the Asian Seas* (pp. 359-376).
1190 Springer International Publishing. https://doi.org/10.1007/978-3-319-94067-0_20
1191 Siegel, H., Stottmeister, I., Reißmann, J., Gerth, M., Jose, C., & Samiaji, J. (2009). Siak River System — East-
1192 Sumatra: Characterisation of sources, estuarine processes, and discharge into the Malacca Strait. *Journal of*
1193 *Marine Systems*, *77*(1), 148-159. https://doi.org/https://doi.org/10.1016/j.jmarsys.2008.12.003
1194 Spencer, R. G. M., Aiken, G. R., Butler, K. D., Dornblaser, M. M., Striegl, R. G., & Hernes, P. J. (2009). Utilizing
1195 chromophoric dissolved organic matter measurements to derive export and reactivity of dissolved organic
1196 carbon exported to the Arctic Ocean: A case study of the Yukon River, Alaska. *Geophysical Research Letters*,
1197 *36*(6). https://doi.org/https://doi.org/10.1029/2008GL036831
1198 Spencer, R. G. M., Butler, K. D., & Aiken, G. R. (2012). Dissolved organic carbon and chromophoric dissolved
1199 organic matter properties of rivers in the USA. *Journal of Geophysical Research: Biogeosciences*, *117*(G3),
1200 n/a-n/a. https://doi.org/10.1029/2011jg001928
1201 Spencer, R. G. M., Hernes, P. J., Ruf, R., Baker, A., Dyda, R. Y., Stubbins, A., & Six, J. (2010). Temporal controls
1202 on dissolved organic matter and lignin biogeochemistry in a pristine tropical river, Democratic Republic of
1203 Congo. *Journal of Geophysical Research: Biogeosciences*, *115*(G3).
1204 https://doi.org/https://doi.org/10.1029/2009JG001180
1205 Spencer, R. G. M., Stubbins, A., Hernes, P. J., Baker, A., Mopper, K., Aufdenkampe, A. K., et al. (2009).
1206 Photochemical degradation of dissolved organic matter and dissolved lignin phenols from the Congo River.
1207 *Journal of Geophysical Research: Biogeosciences*, *114*(G3).
1208 https://doi.org/https://doi.org/10.1029/2009JG000968
1209 Stedmon, C. A., Amon, R. M. W., Rinehart, A. J., & Walker, S. A. (2011). The supply and characteristics of colored
1210 dissolved organic matter (CDOM) in the Arctic Ocean: Pan Arctic trends and differences. *Marine Chemistry*,
1211 *124*(1), 108-118. https://doi.org/https://doi.org/10.1016/j.marchem.2010.12.007
1212 Stedmon, C. A., & Bro, R. (2008). Characterizing dissolved organic matter fluorescence with parallel factor analysis:
1213 a tutorial. *Limnology and Oceanography: Methods*, *6*(11), 572-579. https://doi.org/10.4319/lom.2008.6.572
1214 Stedmon, C. A., & Markager, S. (2005a). Resolving the variability in dissolved organic matter fluorescence in a
1215 temperate estuary and its catchment using PARAFAC analysis. *Limnology and Oceanography*, *50*(2), 686-
1216 697. https://doi.org/10.4319/lo.2005.50.2.0686
1217 Stedmon, C. A., & Markager, S. (2005b). Tracing the production and degradation of autochthonous fractions of
1218 dissolved organic matter by fluorescence analysis. *Limnology and Oceanography*, *50*(5), 1415-1426.
1219 http://www.jstor.org/stable/3597686
1220 Stedmon, C. A., Markager, S., & Bro, R. (2003). Tracing dissolved organic matter in aquatic environments using a
1221 new approach to fluorescence spectroscopy. *Marine Chemistry*, *82*(3), 239-254.
1222 https://doi.org/https://doi.org/10.1016/S0304-4203(03)00072-0
1223 Stedmon, C. A., & Nelson, N. B. (2015). Chapter 10 - The Optical Properties of DOM in the Ocean. In D. A. Hansell
1224 & C. A. Carlson (Eds.), *Biogeochemistry of Marine Dissolved Organic Matter (Second Edition)* (pp. 481-
1225 508). Academic Press. https://doi.org/https://doi.org/10.1016/B978-0-12-405940-5.00010-8
1226 Su, J., Cai, W.-J., Brodeur, J., Hussain, N., Chen, B., Testa, J. M., et al. (2020). Source partitioning of oxygen-
1227 consuming organic matter in the hypoxic zone of the Chesapeake Bay. *Limnology and Oceanography*, *65*(8),
1228 1801-1817. https://doi.org/https://doi.org/10.1002/lno.11419
1229 Su, J., Dai, M., He, B., Wang, L., Gan, J., Guo, X., et al. (2017). Tracing the origin of the oxygen-consuming organic
1230 matter in the hypoxic zone in a large eutrophic estuary: the lower reach of the Pearl River Estuary, China.
1231 *Biogeosciences*, *14*(18), 4085-4099. https://doi.org/10.5194/bg-14-4085-2017
1232 Susanto, R. D., Wei, Z., Adi, T. R., Zheng, Q., Fang, G., Fan, B., et al. (2016). Oceanography Surrounding Krakatau
1233 Volcano in the Sunda Strait, Indonesia. *Oceanography*, *29*(2), 264-272.
1234 http://www.jstor.org/stable/24862689
1235 Urtizberea, A., Dupont, N., Rosland, R., & Aksnes, D. L. (2013). Sensitivity of euphotic zone properties to CDOM
1236 variations in marine ecosystem models. *Ecological Modelling*, *256*, 16-22.
1237 https://doi.org/https://doi.org/10.1016/j.ecolmodel.2013.02.010
1238 Vähätalo, A. V., & Zepp, R. G. (2005). Photochemical Mineralization of Dissolved Organic Nitrogen to Ammonium
1239 in the Baltic Sea. *Environmental Science & Technology*, *39*(18), 6985-6992.
1240 https://doi.org/10.1021/es050142z
1241 van Maren, D. S., & Gerritsen, H. (2012). Residual flow and tidal asymmetry in the Singapore Strait, with implications
1242 for resuspension and residual transport of sediment. *Journal of Geophysical Research: Oceans*, *117*(C4).
1243 https://doi.org/https://doi.org/10.1029/2011JC007615

Vantrepotte, V., Danhiez, F.-P., Loisel, H., Ouillon, S., Mériaux, X., Cauvin, A., & Dessailly, D. (2015). CDOM-DOC relationship in contrasted coastal waters: implication for DOC retrieval from ocean color remote sensing observation. *Optics Express*, *23*(1), 33-54. https://doi.org/10.1364/OE.23.000033

Vione, D., Lauri, V., Minero, C., Maurino, V., Malandrino, M., Carlotti, M. E., et al. (2009). Photostability and photolability of dissolved organic matter upon irradiation of natural water samples under simulated sunlight. *Aquatic Sciences*, *71*(1), 34-45. https://doi.org/10.1007/s00027-008-8084-3

Walker, S. A., Amon, R. M. W., & Stedmon, C. A. (2013). Variations in high-latitude riverine fluorescent dissolved organic matter: A comparison of large Arctic rivers. *Journal of Geophysical Research: Biogeosciences*, *118*(4), 1689-1702. https://doi.org/https://doi.org/10.1002/2013JG002320

Ward, C. P., Nalven, S. G., Crump, B. C., Kling, G. W., & Cory, R. M. (2017). Photochemical alteration of organic carbon draining permafrost soils shifts microbial metabolic pathways and stimulates respiration. *Nature Communications*, *8*(1), 772. https://doi.org/10.1038/s41467-017-00759-2

Weishaar, J. L., Aiken, G. R., Bergamaschi, B. A., Fram, M. S., Fujii, R., & Mopper, K. (2003). Evaluation of specific ultraviolet absorbance as an indicator of the chemical composition and reactivity of dissolved organic carbon. *Environ Sci Technol*, *37*(20), 4702-4708. https://doi.org/10.1021/es030360x

Wilske, C., Herzsprung, P., Lechtenfeld, O. J., Kamjunke, N., & von Tümpling, W. (2020). Photochemically Induced Changes of Dissolved Organic Matter in a Humic-Rich and Forested Stream. *Water*, *12*(2), 331. https://www.mdpi.com/2073-4441/12/2/331

Wit, F., Rixen, T., Baum, A., Pranowo, W. S., & Hutahaean, A. A. (2018). The Invisible Carbon Footprint as a hidden impact of peatland degradation inducing marine carbonate dissolution in Sumatra, Indonesia. *Scientific Reports*, *8*(1), 17403. https://doi.org/10.1038/s41598-018-35769-7

Yamashita, Y., Fichot, C. G., Shen, Y., Jaffé, R., & Benner, R. (2015). Linkages among fluorescent dissolved organic matter, dissolved amino acids and lignin-derived phenols in a river-influenced ocean margin [Original Research]. *Frontiers in Marine Science*, *2*(92). https://doi.org/10.3389/fmars.2015.00092

Yamashita, Y., Jaffé, R., Maie, N., & Tanoue, E. (2008). Assessing the dynamics of dissolved organic matter (DOM) in coastal environments by excitation emission matrix fluorescence and parallel factor analysis (EEM-PARAFAC). *Limnology and Oceanography*, *53*(5), 1900-1908. https://doi.org/10.4319/lo.2008.53.5.1900

Yamashita, Y., & Tanoue, E. (2003). Chemical characterization of protein-like fluorophores in DOM in relation to aromatic amino acids. *Marine Chemistry*, *82*(3), 255-271. https://doi.org/https://doi.org/10.1016/S0304-4203(03)00073-2

Yang, L., & Hur, J. (2014). Critical evaluation of spectroscopic indices for organic matter source tracing via end member mixing analysis based on two contrasting sources. *Water Research*, *59*, 80-89. https://doi.org/https://doi.org/10.1016/j.watres.2014.04.018

Ye, F., Guo, W., Wei, G., & Jia, G. (2018). The Sources and Transformations of Dissolved Organic Matter in the Pearl River Estuary, China, as Revealed by Stable Isotopes. *Journal of Geophysical Research: Oceans*, *123*(9), 6893-6908. https://doi.org/https://doi.org/10.1029/2018JC014004

Zeebe, R. E., & Wolf-Gladrow, D. (2001). *CO2 in seawater: equilibrium, kinetics, isotopes*. Gulf Professional Publishing.

Zhou, Y., Evans, C. D., Chen, Y., Chang, K. Y. W., & Martin, P. (2021). Extensive Remineralization of Peatland-Derived Dissolved Organic Carbon and Ocean Acidification in the Sunda Shelf Sea, Southeast Asia. *Journal of Geophysical Research: Oceans*, *126*(6), e2021JC017292. https://doi.org/https://doi.org/10.1029/2021JC017292

Zhou, Y., Martin, P., & Müller, M. (2019). Composition and cycling of dissolved organic matter from tropical peatlands of coastal Sarawak, Borneo, revealed by fluorescence spectroscopy and parallel factor analysis. *Biogeosciences*, *16*(13), 2733-2749. https://doi.org/10.5194/bg-16-2733-2019

Zhu, Z. Y., Oakes, J., Eyre, B., Hao, Y., Sia, E. S. A., Jiang, S., et al. (2020). The nonconservative distribution pattern of organic matter in the Rajang, a tropical river with peatland in its estuary. *Biogeosciences*, *17*(9), 2473-2485. https://doi.org/10.5194/bg-17-2473-2020

Zigah, P. K., McNichol, A. P., Xu, L., Johnson, C., Santinelli, C., Karl, D. M., & Repeta, D. J. (2017). Allochthonous sources and dynamic cycling of ocean dissolved organic carbon revealed by carbon isotopes. *Geophysical Research Letters*, *44*(5), 2407-2415. https://doi.org/https://doi.org/10.1002/2016GL071348

Zsolnay, A., Baigar, E., Jimenez, M., Steinweg, B., & Saccomandi, F. (1999). Differentiating with fluorescence spectroscopy the sources of dissolved organic matter in soils subjected to drying. *Chemosphere*, *38*(1), 45-50. https://doi.org/https://doi.org/10.1016/S0045-6535(98)00166-0

JGR Biogeosciences

Supporting Information for

The validity of optical properties as tracers of terrigenous dissolved organic carbon during extensive remineralization in coastal waters

Yuan Chen[1], Patrick Martin[1], Yongli Zhou[1, †]

[1] Asian School of the Environment, Nanyang Technological University, 639798, Singapore

[†] Present address: Marine Biological Laboratory, Woods Hole, MA 02543, USA

Contents of this file

Introduction

The dataset contains previous data collected from Sarawak in north-western Borneo (Martin et al., 2018; Zhou et al., 2019), monthly data collected in the Singapore Strait, and experimental data for Singapore coastal water and a peatland-draining river water in Sarawak (partly published in Zhou et al. (2021)). Text S1 explains the calculation of the tDOC concentration and remineralized tDOC based on a two-endmember mixing model and a carbon isotope mass balance. Figure S1 shows a map of our study area. Figure S2 shows the derivation and validation of the riverine endmember value of a_{440} obtained from discharge-weighted average of four main rivers located on Sumatra (Siegel et al., 2019; Wit et al., 2018). Figure S3 presents fingerprints of five fluorescent components identified by parallel factor analysis (PARAFAC). Figure S4 shows that there is no relationship between dissolved organic matter optical properties and the extent of tDOC remineralization. Table S1 shows the parameter values used for the isotope mass balance calculation and the corresponding uncertainty calculation. Table S2 presents apparent and actual riverine endmember values from conservative mixing of remaining tDOC, total initial tDOC and timeseries a_{440} in the Singapore Strait, and discharge-weighted average a_{440} from data of four main rivers on Sumatra. Table S3 describes spectral characteristics and possible sources of the five PARAFAC components.

Text S1: Calculations of the remaining tDOC concentration and the amount of remineralized tDOC

S1.1 Remaining tDOC

We used a two-endmember isotope mixing model to calculate the concentration of tDOC in each sample, i.e., remaining tDOC concentration, from measured $\delta^{13}C_{DOC}$ and total DOC concentration. As our samples are the mixture of tDOC and marine DOC (mDOC), the measured DOC concentration and ^{13}C concentration are expressed as equations (Eqs.) S1–3:

$$[\mathbf{DOC}]_{\mathbf{meas}} = [\mathbf{tDOC}] + [\mathbf{mDOC}] \quad \text{(S1)}$$

$$[\mathbf{DO^{13}C}]_{\mathbf{meas}} = [\mathbf{DO^{13}C}]_{\mathbf{tDOC}} + [\mathbf{DO^{13}C}]_{\mathbf{mDOC}} \quad \text{(S2)}$$

$$[\mathbf{DO^{13}C}]_{\mathbf{meas}} = [\mathbf{DOC}]_{\mathbf{meas}} \times \frac{^{13}\mathbf{C}}{^{12}\mathbf{C}+^{13}\mathbf{C}+^{14}\mathbf{C}} \quad \text{(S3)}$$

As ^{12}C accounts for >98.9% of total carbon in the natural environment, we can approximate:

$$\frac{^{13}\mathbf{C}}{^{12}\mathbf{C}+^{13}\mathbf{C}+^{14}\mathbf{C}} \approx \frac{^{13}\mathbf{C}}{^{12}\mathbf{C}} \quad \text{(S4)}$$

$$\frac{^{12}\mathbf{C}}{^{12}\mathbf{C}+^{13}\mathbf{C}+^{14}\mathbf{C}} \approx \mathbf{1} \quad \text{(S5)}$$

Therefore, Eq. S3 is approximated as Eq. S6, in which the $^{13}C/^{12}C$ ratio (denoted as R) in the measured sample are calculated from measured $\delta^{13}C_{DOC}$ (Eq. S7):

$$[\mathbf{DO^{13}C}]_{\mathbf{meas}} \approx [\mathbf{DOC}]_{\mathbf{meas}} \times \mathbf{R}_{\mathbf{meas}} \quad \text{(S6)}$$

$$\mathbf{R}_{\mathbf{meas}} = (\delta^{\mathbf{13}}\mathbf{C}_{\mathbf{DOC-meas}}(‰) \div \mathbf{1000} + \mathbf{1}) \times \mathbf{R}_{\mathbf{VPDB}} \quad \text{(S7)}$$

where the subscript "VPDB" denotes the international standard Vienna Pee Dee Belemnite (R_{VPDB} = 0.01123720, IAEA (1993)).

Likewise, the concentrations of ^{13}C respectively contributed by tDOC and mDOC are approximated as Eqs. S8–9; R_{tDOC} and R_{mDOC} are calculated from $\delta^{13}C_{DOC}$ values of the riverine and marine endmember, respectively (Eqs. S10–11):

$$[\mathbf{DO^{13}C_{tDOC}}] \approx [\mathbf{tDOC}] \times \mathbf{R_{tDOC}} \quad \text{(S8)}$$

$$[\mathbf{DO^{13}C_{mDOC}}] \approx [\mathbf{mDOC}] \times \mathbf{R_{mDOC}} \quad \text{(S9)}$$

$$\mathbf{R_{tDOC}} = (\delta^{\mathbf{13}}\mathbf{C_{DOC-riv}}(‰) \div \mathbf{1000} + \mathbf{1}) \times \mathbf{R_{VPDB}} \quad \text{(S10)}$$

$$\mathbf{R_{mDOC}} = (\delta^{\mathbf{13}}\mathbf{C_{DOC-mar}}(‰) \div \mathbf{1000} + \mathbf{1}) \times \mathbf{R_{VPDB}} \quad \text{(S11)}$$

By applying Eq. S6 and S8–9 to Eq. S2, we have:

$$[\mathbf{DOC}]_{\mathbf{meas}} \times \mathbf{R_{meas}} = [\mathbf{tDOC}] \times \mathbf{R_{tDOC}} + [\mathbf{mDOC}] \times \mathbf{R_{mDOC}} \quad \text{(S12)}$$

Therefore, we calculated tDOC and mDOC concentrations in each sample by solving Eqs. S1, S7 and S10–12.

S1.2 Remineralized tDOC

For DIC, TA and $\delta^{13}C_{DIC}$, deviations between measured values and values predicted for conservative mixing are caused by photosynthesis/remineralization, $CaCO_3$ dissolution/calcification and CO_2 outgassing/uptake, in known stoichiometric proportions (Samanta et al., 2015; Zeebe & Wolf-Gladrow, 2001). Therefore, we firstly calculated the expected values for DIC, TA and $\delta^{13}C_{DIC}$ from conservative mixing and then estimated the amount of carbon that had undergone each biogeochemical processes from the difference between predicted and measured values and the stoichiometry of each process.

The fraction of river water (f_{riv}) and marine water (f_{mar}) was determined from salinity (Eqs. S1–3):

$$\mathbf{f_{mar}} = \mathbf{salinity_{meas}} \div \mathbf{salinity_{mar}} \quad \text{(S13)}$$

$$\mathbf{f_{riv}} = \mathbf{1} - \mathbf{f_{mar}} \quad \text{(S14)}$$

where the subscripts "mar", "riv" and "meas" denote the marine and riverine endmembers, and measured data, respectively.

Expected values for DIC, TA, $DI^{12}C$ and $DI^{13}C$ from conservative mixing were calculated as:

$$\mathbf{Var_{mix} = Var_{riv} \times f_{riv} + Var_{mar} \times f_{mar}} \quad \text{(S15)}$$

where "Var" stands for the variables DIC, TA, $DI^{12}C$ and $DI^{13}C$, and the subscript "mix" denotes values expected from conservative mixing.

To calculate conservative mixing $\delta^{13}C_{DIC}$ values, we followed the approximation in Eqs. S4–5 and S8–11, and riverine and marine endmember values for $DI^{12}C$ and $DI^{13}C$ were calculated from Eqs. S16–17:

$$\mathbf{[DI^{13}C]_{end} \approx [DIC]_{end} \times R_{end}} \quad \text{(S16)}$$

$$\mathbf{[DI^{12}C]_{end} \approx [DIC]_{end} \times 1} \quad \text{(S17)}$$

where the subscript "end" denotes riverine/marine endmembers.

Combined with $[DI^{12}C]_{mix}$ and $[DI^{13}C]_{mix}$ from Eq. S15, $\delta^{13}C_{DIC\text{-}mix}$ was calculated following Eqs. S18–19:

$$\mathbf{R_{mix} = \frac{[DI^{13}C]_{mix}}{[DI^{12}C]_{mix}}} \quad \text{(S18)}$$

$$\delta^{13}\mathbf{C_{DIC-mix}}(‰) = \mathbf{\frac{R_{mix} - R_{VPDB}}{R_{VPDB}} \times 1000} \quad \text{(S19)}$$

Taking all the physical and biogeochemical processes and their stoichiometric effect into account, which can be derived from the slopes in a TA against DIC plot (Zeebe & Wolf-Gladrow, 2001; Zhou et al., 2021), the measured DIC and TA are expressed as:

$$\mathbf{DIC_{meas} = DIC_{mix} + (+1) \times M_{rem} + (+1) \times M_{diss} + (-1) \times M_{outg}} \quad \text{(S20)}$$

$$\mathbf{TA_{meas} = TA_{mix} + (-0.025) \times M_{rem} + (+2) \times M_{diss} + 0 \times M_{outg}} \quad \text{(S21)}$$

where M represents the molar contribution of different processes, and the subscripts "rem", "diss" and "outg" denote tDOC remineralization/primary production, $CaCO_3$ dissolution/production and CO_2 outgassing/uptake, respectively.

The impacts of tDOC remineralization, calcium carbonate dissolution and CO_2 outgassing on $\delta^{13}C_{DIC}$ were estimated according to Samanta et al. (2015):

$$\Delta\boldsymbol{\delta^{13}C_{DIC-rem}} \approx \frac{\mathbf{M_{rem}}}{\mathbf{DIC_{mix}}} \times (\boldsymbol{\delta^{13}C_{tDIC}} - \boldsymbol{\delta^{13}C_{DIC-mix}}) \quad \text{(S22)}$$

$$\Delta\boldsymbol{\delta^{13}C_{DIC-diss}} \approx \frac{\mathbf{M_{diss}}}{\mathbf{DIC_{mix}}} \times (\boldsymbol{\delta^{13}C_{DIC-diss}} - \boldsymbol{\delta^{13}C_{DIC-mix}}) \quad \text{(S23)}$$

$$\Delta\boldsymbol{\delta^{13}C_{DIC-outg}} \approx \frac{\mathbf{-M_{outg}}}{\mathbf{DIC_{mix}}} \times \mathbf{10^3} \times (\boldsymbol{\alpha_{CO_2}} - \mathbf{1}) \quad \text{(S24)}$$

where the symbol "Δ" represents the deviation between measured data and values expected from conservative mixing caused by each process; $\delta^{13}C_{tDIC}$ is the $\delta^{13}C$ of DIC produced by tDOC remineralization, which we take as –32‰ (see Section 2.5.2) $\delta^{13}C_{DIC\text{-}diss}$ is the $\delta^{13}C$ of DIC produced by carbonate dissolution, reported as 0‰ (Samanta et al., 2015; Su et al., 2019); α_{CO2} is the fractionation factor between air and sea surface, and is calculated from the in-situ temperature and the approximation (Rau et al., 1996; Zeebe & Wolf-Gladrow, 2001; Zhou et al., 2021):

$$\boldsymbol{\varepsilon_{CO_2}} = \mathbf{23.644 - 9701.5 \div T(K)} \quad \text{（S25）}$$

$$\boldsymbol{\varepsilon_{CO_2}} \approx \mathbf{10^3} \times \mathbf{ln}\,\boldsymbol{\alpha_{CO_2}} \approx \mathbf{10^3} \times (\boldsymbol{\alpha_{CO_2}} - \mathbf{1}) \quad \text{（S26）}$$

Then, the measured $\delta^{13}C_{DIC}$ is expressed as the combination of physical mixing and these biogeochemical processes:

$$\delta^{\mathbf{13}}\mathbf{C_{DIC-meas}}(‰) = \delta^{\mathbf{13}}\mathbf{C_{DIC-mix}}(‰) + \frac{\mathbf{M_{rem}}}{\mathbf{DIC_{mix}}} \times (\boldsymbol{\delta^{13}C_{tDIC}} - \boldsymbol{\delta^{13}C_{DIC-mix}}) + \frac{\mathbf{M_{diss}}}{\mathbf{DIC_{mix}}} \times$$
$$(\boldsymbol{\delta^{13}C_{DIC-diss}} - \boldsymbol{\delta^{13}C_{DIC-mix}}) + \frac{\mathbf{-M_{outg}}}{\mathbf{DIC_{mix}}} \times \mathbf{10^3} \times (\boldsymbol{\alpha_{CO_2}} - \mathbf{1}) \quad \text{(S27)}$$

By solving Eqs. S20–21 and 27, M_{rem}, M_{diss} and M_{outg} were calculated. Further details of the derivation and approximation can be found in Zhou et al. (2021).

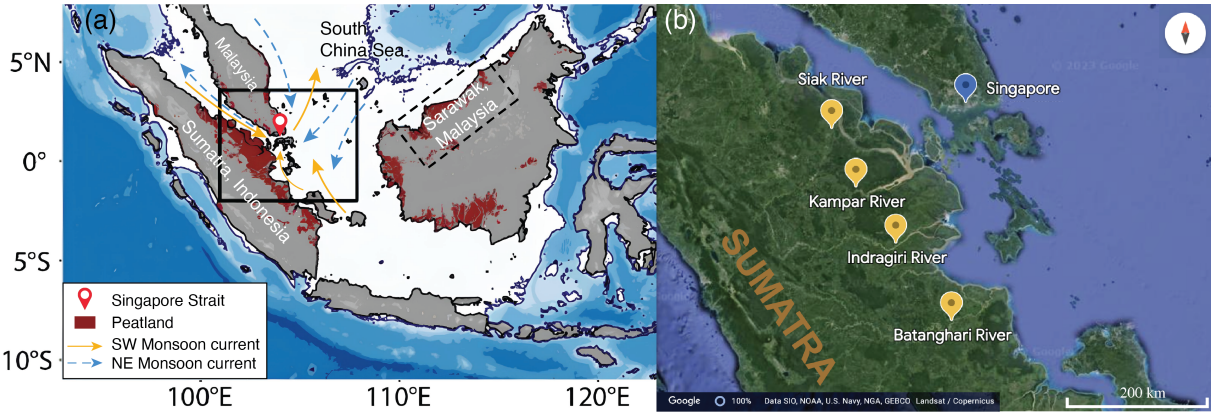

Figure S1. (a) Regional map showing our sampling sites (Singapore Strait and Sarawak) and the monsoon-driven reversal in ocean currents (arrows). (b) Locations of the four peatland-draining rivers (Siak, Kampar, Indragiri and Batanghari) that represent the most plausible main source of tDOC input to the Singapore Strait, and which we used to estimate riverine endmember values.

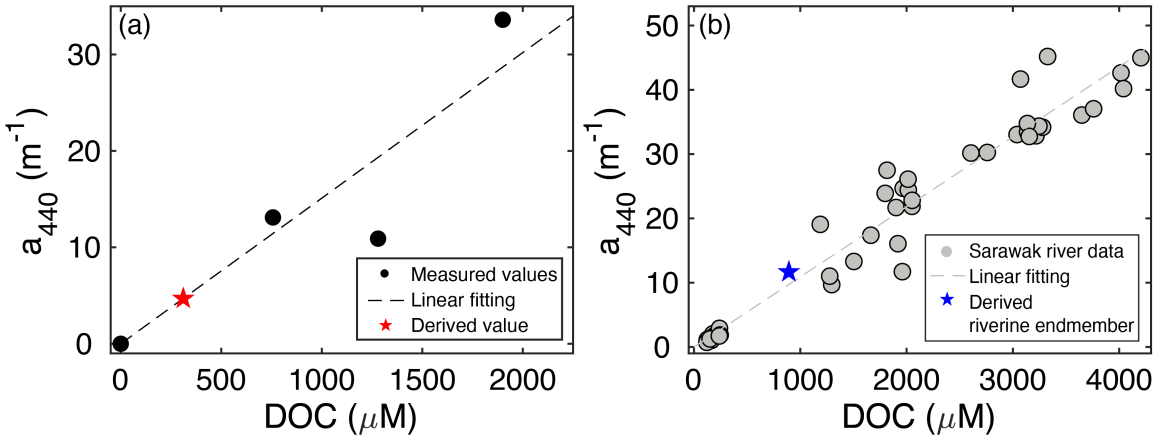

Figure S2. (a) Relationship between average a_{440} and DOC concentration for the four main peatland-draining rivers on Sumatra (Indragiri, Kampar, Siak and Batanghari; data from (Siegel et al., 2019; Wit et al., 2018)). Note that for the Batanghari river there is no published a_{440}, so the Batanghari a_{440} was estimated based on the a_{440}–DOC relationship of the other rivers (red star; relationship forced through the origin). (b) Based on the a_{440} and DOC concentrations in panel (a) and the river discharge data in Wit et al. (2018), we calculated a discharge-weighted average a_{440} and DOC concentration for the four Sumatran rivers as estimated mean riverine endmember values (blue star) for the peatland DOM input to the Singapore Strait. This estimated average riverine a_{440} and DOC for Sumatra falls very close to the relationship of a_{440} to DOC observed for river data measured in Sarawak (Martin et al., 2018).

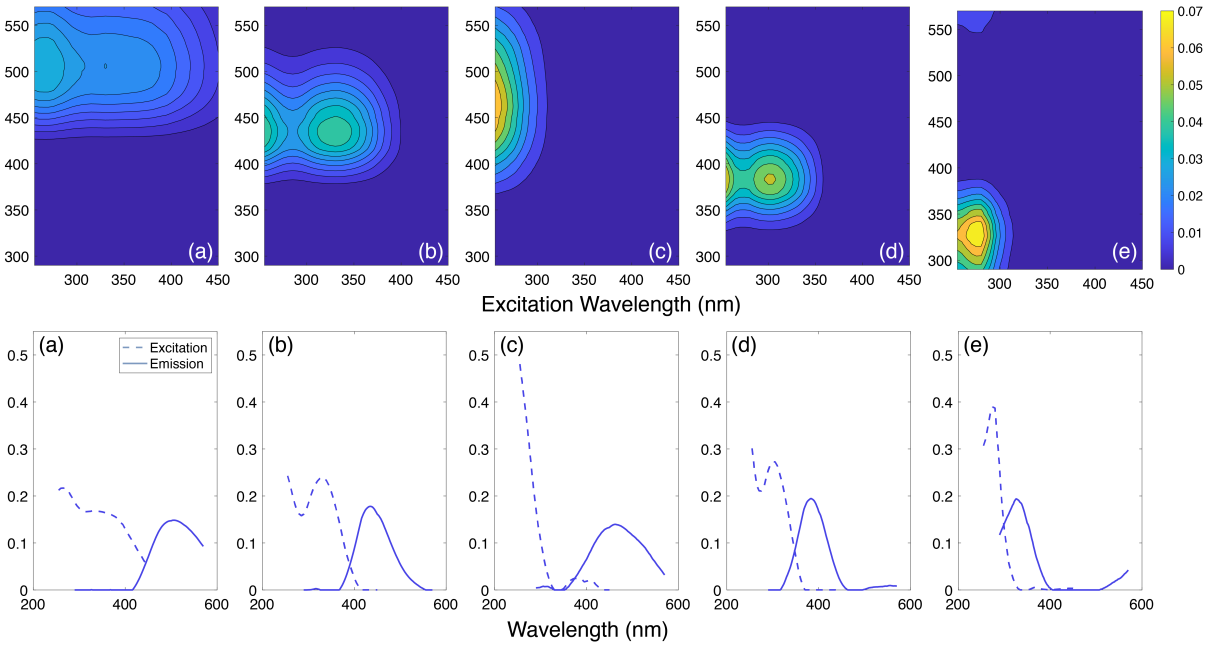

Figure S3. Components revealed by PARAFAC analysis of our combined FDOM dataset; top row shows excitation-emission plots and bottom row shows the corresponding excitation and emission spectra (components 1–5 are ordered left-to-right).

Table S1. Spectral characteristics of the five components identified by PARAFAC analysis for our combined FDOM dataset, and interpretation of possible sources of each compound based on previous literature.

Component	Ex_{max} (nm)	Em_{max} (nm)	Description and probable source	References
C1	265 (330)	506	Soil fulvic acid, common to a wide range of freshwater	(Osburn et al., 2016; Stedmon & Markager, 2005a; Stedmon et al., 2003)
C2	<255 (330)	436	Humic fluorophore group, highest concentration in forest stream and wetlands	(Stedmon & Markager, 2005a; Stedmon et al., 2003)
C3	<255	462	Terrestrial humic substances	(Coble, 1996; Osburn et al., 2016; Stedmon et al., 2003)
C4	<255 (300)	384	Protein-like materials; terrestrial humic materials; possible microbial processed	(Cory & McKnight, 2005; Stedmon & Markager, 2005b; Stedmon et al., 2003; Zhou et al., 2019)
C5	275	326	Non-humic-like materials, autochonomous DOM, tryptophan-like components	(Du et al., 2016; Murphy et al., 2008; Osburn et al., 2016)

Table S2. Endmember values and their uncertainties for all parameters used to calculate the remaining tDOC and total initial tDOC concentrations. Uncertainties for each parameter for the riverine and marine endmembers represent 1 standard deviation and were used to estimate the overall uncertainty for remaining and total initial tDOC using a Monte Carlo Simulation. Analytical uncertainties for each parameter are also given (1 standard deviation).

Parameter	Riverine endmember[a]	Marine endmember	Uncertainty of measurements
Salinity	0	32.56 ± 0.37	± 0.01
DIC (μmol kg^{-1})	453 ± 34	1901 ± 14	± 0.15%
TA (μmol kg^{-1})	310 ± 34	2159 ± 17	± 0.13%
$\delta^{13}C_{DIC}$ (‰)	-15.32 ± 1	-0.23 ± 0.10	± 0.2
$\delta^{13}C_{DOC}$ (‰)	-29 ± 1	-21.39 ± 1.71	± 0.2
$\delta^{13}C_{tDIC}$ (‰)	-32 ± 1	-	-

[a] Discharge-weighted average of published data (Siegel et al., 2019; Wit et al., 2018)

Table S3. Apparent and actual riverine endmember values for remaining and total initial tDOC and for remaining CDOM a_{440} were estimated by extrapolating linear regressions for each parameter versus salinity back to salinity 0, using the Singapore Strait time series data. The total initial a_{440} was estimated as the discharge-weighted average a_{440} from the published river data from Sumatra (see Figure S2).

Parameter used to calculate riverine endmember	Riverine endmember value	Uncertainty	Loss percent
Remaining tDOC (μmol L^{-1})[a]	389	± 97	-
Total initial tDOC (μmol L^{-1})[a]	814	± 133	55.5%
Remaining CDOM (a_{440}, m^{-1})[a]	2.72	± 0.18	-
Total initial CDOM (a_{440}, m^{-1})[b]	11.67	± 0.90	76.5%

[a] Apparent conservative mixing of timeseries data in the Singapore Strait
[b] Discharge-weighted average of four main rivers located on Sumatra (Siegel et al., 2019; Wit et al., 2018)

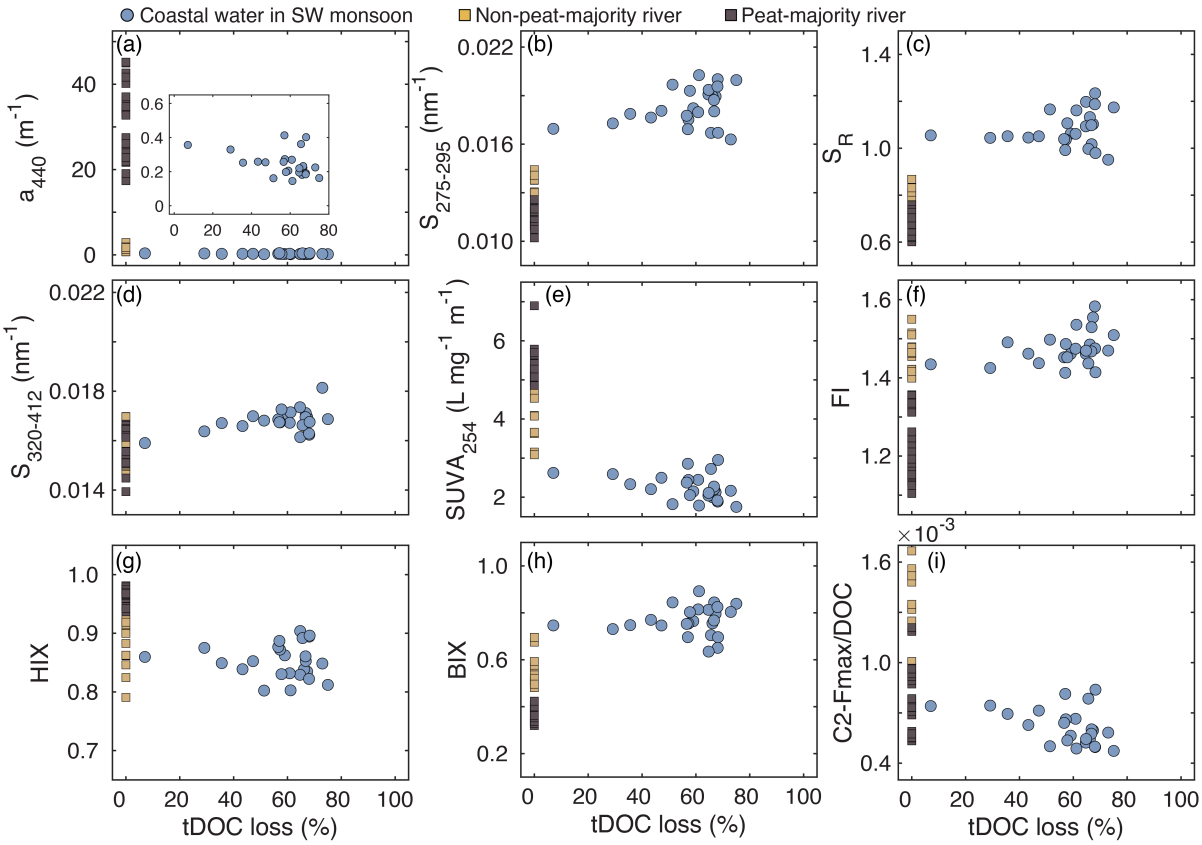

Figure S4. The relationship between optical properties and percentage tDOC remineralization (as calculated from the proportion of remineralized tDOC relative to total initial tDOC based on the carbon stable isotope mass balance). Coastal water data from the Singapore Strait are shown in blue circles (SW Monsoon season only) while Sarawak river data are showed in light and dark brown squares for rivers with, respectively, <50% and >50% peatland coverage in their catchments. We found no significant correlations for the Singapore data, indicating that these optical properties may not be able to quantify the extent of tDOC remineralization.

Data Set S1. Compiled dataset including multi-year time series (from Oct-2017 to Jul-2021) of DOC concentration, stable carbon isotope composition, and optical properties collected in the Singapore Strait, environmental data collected from three expeditions in Sarawak, Borneo and experimental data from photo- and biodegradation incubations for peatland-draining river water and coastal seawater.

References

Coble, P. G. (1996). Characterization of marine and terrestrial DOM in seawater using excitation-emission matrix spectroscopy. Marine Chemistry, 51(4), 325-346. https://doi.org/https://doi.org/10.1016/0304-4203(95)00062-3

Cory, R. M., & McKnight, D. M. (2005). Fluorescence spectroscopy reveals ubiquitous presence of oxidized and reduced quinones in dissolved organic matter. Environmental Science & Technology, 39(21), 8142-8149. https://doi.org/10.1021/es0506962

Du, Y., Zhang, Y., Chen, F., Chang, Y., & Liu, Z. (2016). Photochemical reactivities of dissolved organic matter (DOM) in a sub-alpine lake revealed by EEM-PARAFAC: An insight into the fate of allochthonous DOM in alpine lakes affected by climate change. Science of The Total Environment, 568, 216-225. https://doi.org/https://doi.org/10.1016/j.scitotenv.2016.06.036

Martin, P., Cherukuru, N., Tan, A. S. Y., Sanwlani, N., Mujahid, A., & Müller, M. (2018). Distribution and cycling of terrigenous dissolved organic carbon in peatland-draining rivers and coastal waters of Sarawak, Borneo. Biogeosciences, 15(22), 6847-6865. https://doi.org/10.5194/bg-15-6847-2018

Murphy, K. R., Stedmon, C. A., Waite, T. D., & Ruiz, G. M. (2008). Distinguishing between terrestrial and autochthonous organic matter sources in marine environments using fluorescence spectroscopy. Marine Chemistry, 108(1), 40-58. https://doi.org/https://doi.org/10.1016/j.marchem.2007.10.003

Osburn, C. L., Boyd, T. J., Montgomery, M. T., Bianchi, T. S., Coffin, R. B., & Paerl, H. W. (2016). Optical proxies for terrestrial dissolved organic matter in estuaries and coastal Waters [Original Research]. Frontiers in Marine Science, 2(127). https://doi.org/10.3389/fmars.2015.00127

Rau, G. H., Riebesell, U., & Wolf-Gladrow, D. (1996). A model of photosynthetic 13C fractionation by marine phytoplankton based on diffusive molecular CO2 uptake. Marine Ecology Progress Series, 133, 275-285. https://www.int-res.com/abstracts/meps/v133/p275-285/

Samanta, S., Dalai, T. K., Pattanaik, J. K., Rai, S. K., & Mazumdar, A. (2015). Dissolved inorganic carbon (DIC) and its δ13C in the Ganga (Hooghly) River estuary, India: Evidence of DIC generation via organic carbon degradation and carbonate dissolution. Geochimica et Cosmochimica Acta, 165, 226-248. https://doi.org/https://doi.org/10.1016/j.gca.2015.05.040

Siegel, H., Gerth, M., Stottmeister, I., Baum, A., & Samiaji, J. (2019). Remote sensing of coastal discharge of SE Sumatra (Indonesia). In V. Barale & M. Gade (Eds.), Remote Sensing of the Asian Seas (pp. 359-376). Springer International Publishing. https://doi.org/10.1007/978-3-319-94067-0_20

Stedmon, C. A., & Markager, S. (2005a). Resolving the variability in dissolved organic matter fluorescence in a temperate estuary and its catchment using PARAFAC analysis. Limnology and Oceanography, 50(2), 686-697. https://doi.org/10.4319/lo.2005.50.2.0686

Stedmon, C. A., & Markager, S. (2005b). Tracing the production and degradation of autochthonous fractions of dissolved organic matter by fluorescence analysis. Limnology and Oceanography, 50(5), 1415-1426. http://www.jstor.org/stable/3597686

Stedmon, C. A., Markager, S., & Bro, R. (2003). Tracing dissolved organic matter in aquatic environments using a new approach to fluorescence spectroscopy. Marine Chemistry, 82(3), 239-254. https://doi.org/https://doi.org/10.1016/S0304-4203(03)00072-0

Su, J., Cai, W.-J., Hussain, N., Brodeur, J., Chen, B., & Huang, K. (2019). Simultaneous determination of dissolved inorganic carbon (DIC) concentration and stable isotope (δ13C-DIC) by Cavity Ring-Down Spectroscopy: Application to study carbonate dynamics in the Chesapeake Bay. Marine Chemistry, 215, 103689. https://doi.org/https://doi.org/10.1016/j.marchem.2019.103689

Wit, F., Rixen, T., Baum, A., Pranowo, W. S., & Hutahaean, A. A. (2018). The Invisible Carbon Footprint as a hidden impact of peatland degradation inducing marine carbonate dissolution in Sumatra, Indonesia. Scientific Reports, 8(1), 17403. https://doi.org/10.1038/s41598-018-35769-7

Zeebe, R. E., & Wolf-Gladrow, D. (2001). CO2 in seawater: equilibrium, kinetics, isotopes. Gulf Professional Publishing.

Zhou, Y., Evans, C. D., Chen, Y., Chang, K. Y. W., & Martin, P. (2021). Extensive Remineralization of Peatland-Derived Dissolved Organic Carbon and Ocean Acidification in the Sunda Shelf Sea, Southeast Asia. Journal of Geophysical Research: Oceans, 126(6), e2021JC017292. https://doi.org/https://doi.org/10.1029/2021JC017292

Zhou, Y., Martin, P., & Müller, M. (2019). Composition and cycling of dissolved organic matter from tropical peatlands of coastal Sarawak, Borneo, revealed by fluorescence spectroscopy and parallel factor analysis. Biogeosciences, 16(13), 2733-2749. https://doi.org/10.5194/bg-16-2733-2019